Evaluation of ecosystem dynamics, plant geography and terrestrial carbon cycling in the LPJ dynamic global vegetation model

Stephen Sitch, B. Smith, I. Colin Prentice, A. Arneth, Alberte Bondeau, Wolfgang Cramer, J. O. Kaplan, S. Levis, Wolfgang Lucht, M. T. Sykes, et al.

Evaluation of ecosystem dynamics, plant geography and terrestrial carbon cycling in the LPJ dynamic global vegetation model

S. Sitch[a], B. Smith[b], I.C. Prentice[c], A. Arneth[c,1], A. Bondeau[a], W. Cramer[a], J. O. Kaplan[d], S. Levis[c,a,2], W. Lucht[a], M.T. Sykes[b], K. Thonicke[a] and S. Venevsky[a]

[a]Potsdam Institut für Klimafolgenforschung (PIK) e.V., Telegrafenberg, PO Box 601203, D-14412 Potsdam, Germany,
[b]Departmentof Physical Geography and Ecosystems Analysis, SoÈlvegatan 13, University of Lund, S-22362 Lund, Sweden,
[c]Max Planck Institutefor Biogeochemistry, PO Box 100164, D-07701 Jena, Germany,
[d]Canadian Centre of Climate Modelling and Analysis, University ofVictoria, PO Box 1700, STN, CSC, Victoria, B.C., V8W 2Y2, Canada

The Lund–Potsdam–Jena Dynamic Global Vegetation Model (LPJ) combines process-based, large-scale representations of terrestrial vegetation dynamics and land-atmosphere carbon and water exchanges in a modular framework. Features include feedback through canopy conductance between photosynthesis and transpiration and interactive coupling between these 'fast' processes and other ecosystem processes including resource competition, tissue turnover, population dynamics, soil organic matter and litter dynamics and fire disturbance. Ten plants functional types (PFTs) are differentiated by physiological, morphological, phenological, bioclimatic and fire-response attributes. Resource competition and differential responses to fire between PFTs influence their relative fractional cover from year to year. Photosynthesis, evapotranspiration and soil water dynamics are modelled on a daily time step, while vegetation structure and PFT population densities are updated annually.

Simulations have been made over the industrial period both for specific sites where field measurements were available for model evaluation, and globally on a 0.5°° × 0.5°° grid. Modelled vegetation patterns are consistent with observations, including remotely sensed vegetation structure and phenology. Seasonal cycles of net ecosystem exchange and soil moisture compare well with local measurements. Global carbon exchange fields used as input to an atmospheric tracer transport model (TM2) provided a good fit to observed seasonal cycles of CO_2 concentration at all latitudes. Simulated inter-annual variability of the global terrestrial carbon balance is in phase with and comparable in amplitude to observed variability in the growth rate of atmospheric CO_2. Global terrestrial carbon and water cycle parameters (pool sizes and fluxes) lie within their accepted ranges. The model is being used to study past, present and future terrestrial ecosystem dynamics, biochemical and biophysical interactions between ecosystems and the atmosphere, and as a component of coupled Earth system models.

Keywords: biogeochemistry, carbon cycle, CO_2 , dynamic global vegetation model, ecosystemdynamics, terrestrial biosphere model

Correspondence: Stephen Sitch, Potsdam Institut für Klimafolgenforschung (PIK) e.V., Telegrafenberg, PO Box 60 12 03, D-144 12 Potsdam, Germany, fax +49 331 288 2640, e-mail: sitch@pik-potsdam.de
[1]Present address: Max Planck Institute for Meteorology, Bundesstrasse 55, D-20146 Hamburg, Germany
[2]Present address: National Center for Atmospheric Research, PO Box 3000, Boulder, CO 80307, USA

Introduction

The terrestrial biosphere plays a pivotal role in the Earth system through biophysical interactions and biogeochemical exchanges with the atmosphere and oceans (e.g. Foley *et al*., 1994; Prentice *et al*., 2000). In particular, terrestrial ecosystems are a dynamic component of the global carbon cycle. More than one third of the CO_2 in the

atmosphere is exchanged annually with the terrestrial biosphere by passage through stomata into leaves and solution in leaf water (Farquhar *et al*., 1993; Ciais *et al*., 1997), and about half of this amount is fixed in photosynthesis. Terrestrial ecosystem processes also regulate the exchange of energy, water and momentum between the atmosphere and land. The need to better understand and quantify the global behaviour of terrestrial ecosystems as a major 'actor' in Earth system dynamics has been driving the development of global terrestrial biogeochemistry and biogeography models since the late 1980s, and more recently the development of fully integrated dynamic global vegetation models (DGVMs) (Prentice *et al*., 1989; Steffen *et al*., 1992; Cramer *et al*., 2001).

Human activities are perturbing the global carbon cycle by fossil-fuel burning and land use changes, as most recently summarized by Prentice *et al*. (2001). Many studies have been conducted with terrestrial biogeochemistry models to assess potential effects of changes in atmospheric CO_2 concentration and climate on global carbon storage in vegetation and soils (e.g. Melillo *et al*., 1993; Friedlingstein *et al*., 1995; Cao & Woodward, 1998). Equilibrium biogeography models (Prentice *et al*., 1992; Neilson, 1995; Haxeltine & Prentice, 1996a) have been used to provide projections of future vegetation distribution, partly for use as input to biogeochemistry models that could not simulate transitions between vegetation types (Foley, 1995; VEMAP, 1995). These hybrid-modelling studies did not consider transient effects of vegetation structural changes, which might interact with terrestrial carbon dynamics in highly nonlinear ways. Dynamic global vegetation models combine representations of biogeochemical processes with representations of processes contributing to the dynamics of vegetation structure and composition and thus ultimately to changes in ecosystem geography. Vegetation dynamic processes have been treated in so-called gap models (Botkin *et al*., 1972; Shugart, 1984; Leemans & Prentice, 1989; Prentice & Leemans, 1990; Pacala *et al*., 1993; Prentice *et al*., 1993; Fulton & Prentice, 1997; Bugmann & Cramer, 1998; Smith *et al*., 2001) but these require considerable generalization to be applicable in a global context. Several DGVMs have now been independently developed (Foley *et al*., 1996; Brovkin *et al*., 1997; Friend *et al*., 1997; Cox *et al*., 1998; Woodward *et al*., 2000) and applied to problems of the global carbon cycle (Prentice *et al*., 2000; Cramer *et al*., 2001; McGuire *et al*., 2001; Prentice *et al*., 2001) and climate change (Brovkin *et al*., 1999; Cox *et al*., 2000). Foley *et al*. (1996, 1998) first tackled the problem of physically coupling a DGVM to an atmospheric general circulation model. Cox *et al*. (2000) presented the first simulations with a DGVM fully coupled via physical and carbon exchanges among the oceans, atmosphere and land.

The existing DGVMs differ in their degree of complexity and suitability for different tasks. The Lund–Potsdamn–Jena Model (LPJ) has been developed as a DGVM of intermediate complexity with a broad range of potential applications to global problems. Three major considerations have guided its development:

1. Process-based yet computationally efficient representation of land-atmosphere coupling, building on earlier work in an equilibrium biogeography modelling context by Haxeltine *et al.* (1996) and Haxeltine & Prentice (1996a).
2. Explicit inclusion of the major processes of vegetation dynamics, including the role of the natural fire regime, and growth, competition and demographic processes as represented in gap models, albeit in a highly parameterized form suitable for global applications. (A landscape model version (GUESS) (Smith *et al.*, 2001) with identical land-atmosphere coupling but 'gap model' representation of vegetation processes has been developed for local to regional applications).
3. An emphasis on comprehensive evaluation, using the widest possible range of data sets from atmospheric science as well as ecosystem science.

The *Methods* Section of this paper describes the key features of LPJ. In the *Results* Section, the model is evaluated against data sets spanning a wide range of temporal and spatial scales. The *Discussion* outlines the range of current and potential applications of the model.

Methods

Overview

The LPJ–DGVM has adopted many features from the BIOME family of models (Prentice *et al*., 1992; Haxeltine & Prentice, 1996a; Haxeltine *et al*., 1996; Kaplan, 2001). Bioclimatic limits as introduced in BIOME1, later used in BIOME3, have also been adopted in LPJ. Vegetation in a grid cell is described in terms of the fractional coverage of populations of different plant functional types (PFTs). Modellers define PFTs to account, in a very general way, for the variety of structure and function among plants (Smith *et al*., 1997). We define 10 PFTs, of which eight are woody (two tropical, three temperate, three boreal) and two herbaceous (Tables 1 and 2), following similar logic to that used in equilibrium biogeography models of the BIOME family (Prentice *et al*., 1992; Haxeltine & Prentice, 1996a; Haxeltine *et al*., 1996; Kaplan, 2001). In addition to the attributes controlling physiology and dynamics, each PFT is assigned bioclimatic limits which determine whether it can survive

Table 1 PFT parameter values: $z_1$and z_2 are the fraction of fine roots in the upper and lower soil layers, respectively; g_{min} is the minimum canopy conductance; r_{fire} is the fire resistance; a_{leaf} is the leaf longevity; f_{leaf}, $f_{sapwood}$, f_{root} are the leaf, sapwood and fine root turnover times, respectively; $t_{mort,min}$ is the temperature base in the heat damage mortality function and S_{GDD} is the growing degree day requirement to grow full leaf coverage

PFT	W/H*	z_1 (–)	z_2 (–)	g_{min} (mm s^{-1})	r_{fire} (–)	a_{leaf} (yr)	f_{leaf} (yr^{-1})	$f_{sapwood}$ (yr^{-1})	f_{root} (yr^{-1})	$T_{mort,min}$ (°C)	S_{GDD} (°C)
Tropical broad-leaved evergreen (TrBE)	*W*	0.85	0.15	0.5	0.12	2.0	0.5	0.05	0.5	–	–
Tropical broad-leaved raingreen (TrBR)	*W*	0.70	0.30	0.5	0.50	0.5	1.0	0.05	1.0	–	–
Temperate needle-leaved evergreen (TeNE)	*W*	0.70	0.30	0.3	0.12	2.0	0.5	0.05	0.5	–	–
Temperate broad-leaved evergreen (TeBE)	*W*	0.70	0.30	0.5	0.50	1.0	1.0	0.05	1.0	–	–
Temperate broad-leaved summergreen (TeBS)	*W*	0.80	0.20	0.5	0.12	0.5	1.0	0.05	1.0	–	200
Boreal needle-leaved evergreen (BoNE)	*W*	0.90	0.10	0.3	0.12	2.0	0.5	0.05	0.5	23	–
Boreal needle-leaved summergreen (BoNS)	*W*	0.90	0.10	0.5	0.12	0.5	1.0	0.05	1.0	23	100
Boreal broad-leaved summergreen (BoBS)	*W*	0.90	0.10	0.3	0.12	0.5	1.0	0.05	1.0	23	200
Temperate herbaceous (TeH)	*H*	0.90	0.10	0.5	1.00	1.0	1.0	–	0.5	–	100
Tropical herbaceous (TrH)	*H*	0.90	0.10	0.5	1.00	1.0	1.0	–	0.5	–	100

*W = Woody; H = Herbaceous.

Table 2 PFT Bioclimatic limits: $T_{c,min}$ = minimum coldest-month temperature for survival; $T_{c,max}$ = maximum coldest-month temperature for establishment; GDD_{min} = minimum degree-day sum (5 °C base) for establishment; $T_{w-c,min}$ = minimum warmest minus coldest month temperature range

PFT	$T_{c,min}$ (°C)	$T_{c,max}$ (°C)	GDD_{min} (°C)	$T_{w-c,min}$ (°C)
Tropical broad-leaved evergreen	15.5	–	–	–
Tropical broad-leaved raingreen	15.5	–	–	–
Temperate needle-leaved evergreen	−2.0	22.0	900	–
Temperate broad-leaved evergreen	3.0	18.8	1200	–
Temperate broad-leaved summergreen	−17.0	15.5	1200	–
Boreal needle-leaved evergreen	−32.5	−2.0	600	–
Boreal needle-leaved summergreen	–	−2.0	350	43
Boreal broad-leaved summergreen	–	−2.0	350	–
Temperate herbaceous (TeH)	–	15.5	–	–
Tropical herbaceous (TrH)	15.5	–	–	–

and/or regenerate under the climatic conditions prevailing in a particular grid cell at a particular time in the simulation (Table 2) (Sitch, 2000; Venevsky, 2001). Bioclimatic limits follow the BIOME family except the continentality index for the boreal needle-leaved summergreen ($T_{w-c,min}$), which is derived by empirically fitting the distribution of *Larix* spp. to the modern climate (Venevsky, 2001).

Unlike previous models in the family, LPJ also includes explicit representation of vegetation structure, dynamics, competition between PFT populations, and soil biogeochemistry. Figure 1 shows the model logic. The simulation in any grid cell is driven by input of monthly climatology, soil type and atmospheric CO_2 concentration, from which daily potential evapotranspiration and monthly soil temperatures are derived. The seasonal course of leaf phenology is then calculated for summergreen PFTs. Gross primary production (GPP) is calculated for each PFT population applying the coupled photosynthesis and water balance scheme of BIOME3. Maintenance and growth respiration are subtracted, and tissue turnover reduces individual plant biomass, with dead leaf and root tissue entering the litter pools. After subtracting a reproduction cost, the remaining photosynthate is allocated to the C-compartments, satisfying four allometric relationships (see Section *Average individual properties*). Population densities are updated annually based on establishment and mortality. Litter and soil organic matter (SOM) decomposition are driven by seasonal temperatures and soil moisture status.

Average individual properties The fundamental entity simulated in LPJ is the average individual of a PFT. This concept provides a simple way for processes acting

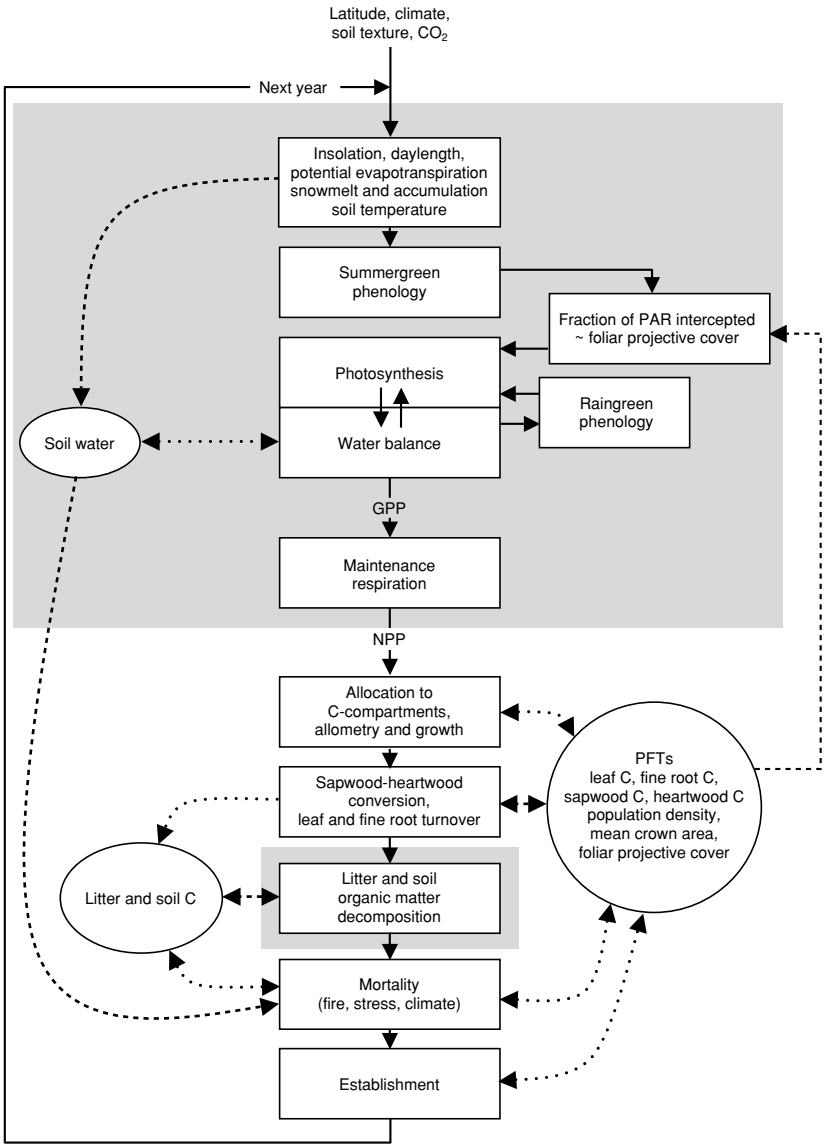

Fig. 1 A flowchart describing the order individual process representations (in boxes), known as modules, are performed (solid lines) in all grid cells, during one simulation year. The dashed lines represent exchange of information between vegetation and soil state variables and the individual modules, with arrows representing the direction of information flow. Modules with a shaded background are called on a daily or monthly time step, the remainder called annually.

at the level of the plant individual to be scaled up to the 'population' over a grid-cell. In principle every higher plant species belongs to a PFT, whose physiology and dynamics are governed by a small set of key attributes. The current PFT classification is rather simple and capable of further development pending progress in PFT classification and characterization (Smith *et al*., 1997). The currently defined PFTs and their attributes are listed in Table 1. A small set of bioclimatic limits constrains PFT survival and regeneration (Table 2). The limits are applied to 20-year running means, not to annual or instantaneous values of the climate variables. This device allowed us to use limit values previously determined for biogeography models (e.g. Prentice *et al*., 1992; Haxeltine & Prentice, 1996a). Each PFT 'population' is characterized by a set of variables describing the state of the average individual, and by the population density (P). For woody PFTs (Table 1) the average individual is defined by its crown area (m^2) and the sizes of four tissue pools (gC): leaf mass (C_{leaf}), sapwood mass ($C_{sapwood}$), heartwood mass ($C_{heartwood}$), and fine root mass (C_{root}). Herbaceous PFTs are treated more simply by a 'big leaf' approximation; population density is arbitrarily set to 1, so that leaf mass and fine root mass represent grid cell area-averages (g C m^{-2}), while sapwood and heartwood mass are undefined.

Four scaling rules define individual physiognomy and constrain biomass allocation among the three living tissue pools (leaves, fine roots and sapwood) in woody plants:

1. The pipe model

$$\mathrm{LA} = k_{\mathrm{la:sa}}\,\mathrm{SA} \tag{1}$$

where LA is the average individual leaf area (m^2), SA (m^2) is the sapwood cross sectional area and $k_{\mathrm{la:sa}}$ is a constant (Table 3). This relationship is based on numerous studies indicating that each unit of leaf area must be supported by a corresponding area of transport tissue (Shinozaki *et al*., 1964a, b; Kaufmann & Troendle, 1981; Waring *et al*., 1982; Ryan, 1989; Robichaud & Methven, 1992; Berninger & Nikinmaa, 1994).

2. Functional balance

A second relationship relates investment in fine roots to investment in leaves and further requires plants in water-limited environments to allocate relatively more resources to fine root biomass. This results in an increased maintenance respiration cost and a loss of potential photosynthetic tissue as the cost of having to acquire water and nutrients (Larcher, 1983; Jackson *et al*., 1996). This relationship is expressed as:

$$C_{\mathrm{leaf}} = \mathrm{lr}_{\mathrm{max}} \cdot \omega \cdot C_{\mathrm{root}} \tag{2}$$

where ω is a value in the range 0–1 representing the current degree of water stress facing the average individual (see Section *Water availability*), while $\mathrm{lr}_{\mathrm{max}}$ is the maximum leaf-to-root mass ratio (Table 3).

3. Stem mechanics

A standard allometry relates vegetation height to stem diameter (e.g. Huang *et al*., 1992).

$$H = k_{\mathrm{allom2}} D^{k_{\mathrm{allom3}}} \tag{3}$$

where k_{allom2}, k_{allom3} are constants (Table 3).

4. Packing constraint

We use a relationship between crown area and stem diameter based on the inversion of Reinecke's rule (Zeide, 1993):

$$\mathrm{CA} = k_{\mathrm{allom1}} D^{k_{\mathrm{rp}}} \tag{4}$$

where k_{allom1} and k_{rp} are constants and $k_{\mathrm{rp}} \approx 1.6$. Crown area is constrained not to exceed a constant, maximum $\mathrm{CA}_{\mathrm{max}}$ (Table 3). Reinicke's rule relates tree density to stem diameter under self-thinning conditions, i.e., neighbourhood-scale survivorship. The inversion used here thus gives the expected relationship between individual crown area and stem diameter, assuming canopy closure but no overlap between crowns of adjacent individuals. Restriction of population density due to self-thinning is modelled in the mortality routine.

A combination of allometries 1–4 implies an increasing sapwood respiration cost with plant height, for a given leaf area. The relative contribution of sapwood respiration to the overall plant respiration increases with height, and is comparable to that of the other tissue respiration costs in tall individuals. Increasing respiration costs eventually restrict individual plant growth.

Other average individual properties

Other properties of the average individual can be derived from the state variables. The leaf area index of an individual is given by

$$\mathrm{LAI}_{\mathrm{ind}} = \frac{C_{\mathrm{leaf}}\,\mathrm{SLA}}{\mathrm{CA}} \tag{5}$$

where SLA is specific leaf area ($m^2\,g\,C^{-1}$). We employ an empirical relationship derived by Reich *et al*. (1997) relating SLA to leaf longevity:

$$\mathrm{SLA} = 2.0 \times 10^{-4} \cdot \frac{e^{6.15}}{(12 a_{\mathrm{leaf}})^{0.46}} \tag{6}$$

where a_{leaf} is a PFT-specific value for leaf longevity in years (Table 1). This is an important relationship with respect to competition between PFTs because it helps to determine whether a deciduous or evergreen strategy is best suited to a given climate.

Leaf area index may be related to foliage projective cover (FPC) (Specht, 1970, 1972, 1981), defined as the area of ground covered by foliage directly above it, by the Lambert–Beer law (Monsi & Saeki, 1953):

$$\mathrm{FPC}_{\mathrm{ind}} = 1 - e^{[-0.5\mathrm{LAI}_{\mathrm{ind}}]} \tag{7}$$

Grid cell properties The overall fractional coverage (FPC) of a PFT in a grid cell is obtained by multiplying average individual FPC with crown area and population density:

$$\mathrm{FPC} = \mathrm{CA} \cdot P \cdot \mathrm{FPC}_{\mathrm{ind}} \tag{8}$$

Consequently, the grid cell is treated as a mosaic divided into fractional coverages of PFTs and bare ground. However, it is assumed that the physical environment of the plants is well mixed, i.e., the PFTs do not occupy discrete blocks, but compete locally for resources. Average individual carbon pools are similarly scaled to the grid cell by multiplying by population density.

Each PFT has an associated above- and below-ground litter pool ($C_{\mathrm{L,ag}}$ and $C_{\mathrm{L,bg}}$, $g\,C\,m^{-2}$). Two soil pools, with 'intermediate' (~30 years) and 'slow' (~1000 years) turnover times, respectively, are defined for the entire grid cell.

Annual vegetation and carbon dynamics The current FPC from Eqn. (8), used as a surrogate for FPAR, the daily leaf phenological status (i.e. fraction of full leaf cover) and climate data are used to calculate GPP for each PFT. This calculation is performed for the middle day of each month and daily values are derived by interpolation between the mid-month values. Maintenance respiration is calculated each simulation day based on the size of the living tissue pools, their assigned C:N ratios (cn) and climate data. Growth respiration, the cost of producing

Table 3 Parameters and constants in model equations

Function	Symbol	Value	Units	Description
Structure	k_{allom1}	100	–	Parameter in Eq. (4)
	k_{allom2}	40	–	Parameter in Eq. (3)
	k_{allom3}	0.5	–	Parameter in Eq. (3)
	$k_{la:sa}$	8000	–	Parameter in Eq. (1)
	cn_{leaf}	29	–	Leaf C:N ratio
	$cn_{sapwood}$	330	–	Sapwood C:N ratio
	cn_{root}	29	–	Root C:N ratio
	k_{rp}	1.6	–	Parameter in Eq. (4)
	CA_{max}	15	m^2	Maximum woody PFT crown area
	lr_{max}	1 (0.75)	–	Leaf-to-root ratio under nonwater stressed conditions (value for herbaceous)
Phenology	T_{base}	5 (2)	°C	Minimum temperature for summergreen PFT leaf growth (value for BoNS)
	ω_{min}	0.35	–	Minimum water stress factor for drought deciduous PFTs
Photosynthesis	pO_2	20.9	kPa	O_2 partial pressure
	p	100.0	kPa	Atmospheric pressure
	θ	0.7	–	Co-limitation (shape) parameter
	$\lambda_{max,c4}$	0.4	–	Optimal c_i/c_a for the tropical herbaceous
	$\lambda_{max,c3}$	0.8	–	Optimal c_i/c_a in C_3 plants (All PFTs except TrH)
	α_{c3}	0.08	–	Intrinsic quantum efficiency of CO_2 uptake in C_3 plants
	α_{c4}	0.053	–	Intrinsic quantum efficiency of CO_2 uptake in C_4 plants
	a_{c3}	0.015	–	Leaf respiration as a fraction of Rubisco capacity in C_3 plants
	a_{c4}	0.02	–	Leaf respiration as a fraction of Rubisco capacity in C_4 plants
Plant Respiration	r	0.066 (0.011)	$g\,C\,g\,N^{-1}\,d^{-1}$	Tissue respiration rate at 10 °C (value for TrBE, TrBR)
Water Balance	α_m	1.4	–	Empirical constant in the evaporative demand function
	g_m	5.0	–	Empirical constant in the evaporative demand function
	E_{max}	5.0	$mm\,d^{-1}$	Maximum transpiration rate
	k_{melt}	3.0	$mm\,°C^{-1}\,d^{-1}$	Rate of snow melt
Mortality	k_{mort1}	0.01	yr^{-1}	Asymptotic maximum mortality rate
	k_{mort2}	0.3	–	Parameter in Eq. (32)
	$fuel_{min}$	200.0	$g\,C\,m^{-2}$	Minimum fuel load for fire spread
	m_e	0.3 (0.2)	–	Litter moisture of extinction (value for herbaceous PFTs)
	r_{fire}	0.12 (0.5)	–	Fire resistance (value for TrBr & TeBE PFTs)
Establishment	est_{max}	0.24	m^{-2}	Maximum sapling establishment rate
	$prec_{min}$	100	$mm\,yr^{-1}$	Minimum annual precipitation for successful sapling establishment
Soil and litter decomposition	f_{air}	0.7	–	Fraction of the decomposed litter emitted as CO_2 to the atmosphere
	f_{inter}	0.985	–	Fraction of soil-bound decomposed litter entering the intermediate soil pool
	f_{slow}	0.015	–	Fraction of soil-bound decomposed litter entering the slow soil pool
	τ_{litter}	2.86	yr	Litter turnover time at 10 °C
	τ_{inter}	33.3	yr	Intermediate soil pool turnover time at 10 °C
	τ_{slow}	1000.0	yr	Slow soil pool turnover time at 10 °C

new tissues, is taken as a fraction of net primary production (NPP). Subtracting maintenance and growth respiration from GPP gives NPP for each PFT. After subtracting an annual reproduction cost from NPP the remaining carbon is available for producing new tissue and is allocated to the living tissue pools of the PFT average individual in such a way as to satisfy the four scaling rules (Eqns 1–4). Tissue pools are also updated annually to account for tissue senescence/turnover (based on assigned turnover times) with carbon entering

the litter (for leaves and fine roots) or (for sapwood) the nonliving heartwood pool.

The sum among PFTs of grid cell FPC is constrained to a maximum value of unity. If tissue growth in a particular year leads to a grid cell FPC sum greater than unity, herbaceous PFT biomass is first reduced (representing the competitive dominance of the taller-growing woody PFT's). If the grid cell FPC sum for woody vegetation exceeds an arbitrary limit of 0.95, woody PFT population is reduced, representing self-thinning. Additional mortality (reduction in population density) can result from depressed growth efficiency, heat stress, negative NPP and when a PFT's bioclimatic limits are exceeded.

The number of new individuals established annually is the product of the PFT-specific potential establishment rate and the fraction of the grid cell currently devoid of woody vegetation, i.e., areas sufficiently illuminated to allow sapling growth. Whether a particular PFT can establish depends also on available soil moisture and bioclimatic limits.

Phenology

Each woody PFT is assigned an evergreen, summergreen or raingreen phenology. Under water- or temperature-limited conditions herbaceous PFTs adopt a raingreen or summergreen phenology, respectively; otherwise, they are treated as evergreens.

Evergreen PFTs maintain constant leaf coverage over the year, and are assigned leaf longevities (a_{leaf}) ≥ 1 year (see Table 1).

For summergreen PFTs, leaf-phenological status (ϕ), updated daily, is defined as the current fraction of this year's maximum leaf coverage. Budburst occurs when daily temperature (T_{d}) exceeds a minimum base temperature (T_{base}). Leaf cover then increases in proportion to the accumulated heat sum (degree-days above T_{base}) until a PFT-specific limit for this heat sum (S_{GDD}) is reached (Table 1). Leaf senescence occurs once daily temperatures again fall below T_{base}.

Maximum leaf coverage for raingreen PFTs is maintained so long as the water stress factor, ω (see below) remains above a threshold value of 0.35. Leaf senescence occurs if ω falls below 0.35.

Production

Water availability Soil hydrology is modelled following the semi-empirical approach of Haxeltine & Prentice (1996a), which was simplified, from the model developed by Neilson (1995). Two soil layers of fixed thickness (0.5 m upper and 1 m lower) are defined. The water content of each layer is updated daily taking into account snowmelt, percolation, rainfall, evapotranspiration and runoff. Precipitation falls as rain or snow depending on whether the daily air temperature is above or below $-2\,^{\circ}$C. Above this threshold the snow pack begins to melt at a maximum rate of

$$\mathrm{melt} = (T_{\mathrm{d}} + 2)\; k_{\mathrm{melt}} \tag{9}$$

where T_{d} is the daily air temperature in °C and k_{melt} is a constant (Table 3). Daily percolation from the upper to the lower soil layer is calculated using the empirical relationship of Neilson (1995),

$$\mathrm{perc} = k_{\mathrm{perc}} W_1^2 \tag{10}$$

where k_{perc} represents the soil texture dependent percolation rate (mm d^{-1}) at field capacity (Table 4) and W_1 is the volumetric water content of the upper layer expressed as a fraction of its available water holding capacity. Surface runoff and drainage are calculated as the excess water above field capacity in the upper and lower soil layers, respectively. Plant functional types differ in their rooting strategy, woody PFTs having a smaller fraction of their

Table 4 Soil Parameters (H_{max} is the volumetric water holding capacity (WHC) at field capacity minus WHC at wilting point, expressed as a fraction of soil layer depth) k_{perc} is the percolation rate field capacity; k_0, k_{15} and k_{100} are the soil thermal diffusivities at 0%, 15% and 100% soil water contents, respectively

Texture-type	k_{perc} (mm d^{-1})	H_{max} (–)	k_0 (mm^2 s^{-1})	k_{15} (mm^2 s^{-1})	k_{100} (mm^2 s^{-1})
Coarse	5.0	0.110	0.2	0.800	0.4
Medium	4.0	0.150	0.2	0.650	0.4
Fine, nonvertisol	3.0	0.120	0.2	0.500	0.4
Medium-coarse	4.5	0.130	0.2	0.725	0.4
Fine-coarse	4.0	0.115	0.2	0.650	0.4
Fine-medium	3.5	0.135	0.2	0.575	0.4
Fine-medium-coarse	4.0	0.127	0.2	0.650	0.4
Organic	9.0	0.300	0.1	0.100	0.1
Fine, vertisol	0.2	0.100	0.2	0.500	0.4

roots in the upper soil layer compared with herbaceous plants. Competition between PFTs for water resources is therefore implicit in the water balance routine.

Daily evapotranspiration is calculated for each PFT as the minimum of a plant- and soil-limited supply function (E_{supply}) and the atmospheric demand (E_{demand}):

$$\text{AET} = \min\left[E_{\text{supply}}, E_{\text{demand}}\right] \tag{11}$$

E_{supply} is the product of plant root-weighted soil moisture availability and a maximum transpiration rate, $E_{\max}$ (Table 3). E_{demand} is calculated following Monteith's (Monteith, 1995; Haxeltine & Prentice, 1996a) empirical relation between evaporation efficiency and surface conductance,

$$E_{\text{demand}} = E_{\text{pot}}\ \alpha_{\text{m}}\left[1 - \exp\left(\frac{-g_{\text{pot}}\phi}{g_{\text{m}}}\right)\right] \tag{12}$$

where E_{pot} is the equilibrium evapotranspiration rate calculated from latitude, temperature and fractional sunshine hours, using a standard method based on the Prescott equation and a similar approximation for longwave radiation (Prentice *et al*., 1993); g_{pot} is the nonwater-stressed potential canopy conductance calculated by the photosynthesis routine (see below), and g_{m} and α_{m} are empirical parameters (Monteith, 1995; Table 3).

The water stress factor (ω) is calculated for each PFT as

$$\omega = \min\left\{1,\ \frac{E_{\text{supply}}}{E_{\text{demand}}}\right\} \tag{13}$$

A daily value of ω is used to update phenological status for raingreen PFTs (see Section *Phenology*), and an annual average value is used in calculating this year's leaf to fine root mass ratio for the allocation routine (Eqn. 2).

Photosynthesis A brief overview of the photosynthesis model is presented here; full derivations are given by Haxeltine & Prentice (1996a, b) and Sitch *et al*. (2002, unpublished). The Farquhar photosynthesis model (Farquhar *et al*., 1980; Farquhar & von Caemmerer, 1982), as generalized for global modelling purposes by Collatz *et al*. (1991, 1992), underlies the model. The 'strong optimality' hypothesis (Dewar, 1996; Haxeltine & Prentice, 1996b; Prentice *et al*., 2000) is assumed to apply; the nitrogen content and Rubisco activity of leaves are assumed to vary both seasonally and with canopy position in such a way as to maximize net assimilation at the leaf level. The resulting model has the form of a 'light-use efficiency' model but the underlying theory makes it possible to predict the light-use efficiency from environmental variables. Photosynthesis by plants adopting the C_3 vs. C_4 biochemical pathways are modelled in slightly different ways. For C_3 plants assimilation A_{nd} (g C $\text{m}^{-2}\,\text{day}^{-1}$) is given by

$$A_{\text{nd}} = I_{\text{d}}\left(\frac{c_1}{c_2}\right)\left[c_2 - (2\theta - 1)s - 2(c_2 - \theta s)\sigma_{\text{c}}\right] \tag{14}$$

where I_{d} is the daily integral of absorbed photosynthetically active radiation (PAR) calculated by a standard method (Haxeltine & Prentice, 1996a), including FPAR which is equal to FPC multiplied by phenology status; θ is the shape parameter which specifies the degree of colimitation by light and Rubisco activity (Haxeltine & Prentice, 1996a, b); and the terms σ_{c}, s, c_1 and c_2 are given by:

$$\sigma_{\text{c}} = \left[1 - \frac{(c_2 - s)}{(c_2 - \theta s)}\right]^{0.5} \tag{15}$$

$$s = \left(\frac{24}{h}\right)a \tag{16}$$

$$c_1 = \alpha\, f_{\text{temp}}\,\frac{(p_{\text{i}} - \Gamma_*)}{(p_{\text{i}} + 2\Gamma_*)} \tag{17}$$

$$c_2 = \frac{(p_{\text{i}} - \Gamma_*)}{\left(p_{\text{i}} + k_{\text{c}}\left(1 + \frac{p\text{O}_2}{k_{\text{o}}}\right)\right)} \tag{18}$$

where h is the day length in hours; a is a constant (leaf respiration as a fraction of Rubisco capacity; see Table 3); α is effective ecosystem-level quantum efficiency (Table 3); f_{temp} is a PFT-specific temperature inhibition function limiting photosynthesis at low and high temperatures (Larcher, 1983; Sitch *et al*., 2002, unpublished); Γ_* is the CO_2 compensation point given by:

$$\Gamma_* = \frac{p\text{O}_2}{2\tau} \tag{19}$$

where $p\text{O}_2$ is the ambient partial pressure of O_2 (Pa); p_{i} is the intercellular partial pressure of CO_2 (Pa) given by

$$p_{\text{i}} = \lambda p_{\text{a}} \tag{20}$$

where p_{a} is the ambient partial pressure of CO_2 and λ is a parameter with a positive value ≤ 0.8. Parameters $\tau, k_{\text{o}}, k_{\text{c}}$ are kinetic parameters with a Q_{10} dependence on temperature (Brooks & Farquhar, 1985; Collatz *et al*., 1991).

An appropriate simplification of the model (with different values for a and α, $\lambda \leq 0.4$, and saturating p_{i}) is applied for herbaceous plants with C_4 physiology (Haxeltine & Prentice, 1996a). The above equations describe the biochemical dependence of total daily net assimilation on p_{i} and environmental variables.

The daytime assimilation rate A_{dt} is also related to p_{i} through the CO_2 diffusion gradient between the atmosphere and intercellular air spaces:

$$g_{\text{c}} = g_{\min} + \frac{1.6A_{\text{dt}}}{[c_{\text{a}}(1 - \lambda)]} \tag{21}$$

where $g_{\min}$ is a PFT-specific minimum canopy conductance (scaled by FPC) and c_{a} is the ambient mole fraction of CO_2 ($p_a = p \cdot c_{\text{a}}$ where p is atmospheric pressure). A_{dt} is obtained from A_{nd} by addition of nighttime respiration.

Under nonwater-stressed conditions maximum values of λ (0.8 for C_3 plants; 0.4 for C_4 plants) are assumed; and is calculated from Eqn. (14) and g_c is derived from Eq. (21). The value for canopy conductance thus obtained is the potential canopy conductance, g_{pot}, required to derive demand-limited AET in Eqn. (12). If $\omega < 1$ (supply limitation of transpiration), Eqns (12), (14) and (21) are solved simultaneously to yield values of λ and g_c consistent with the transpiration rate. Annual GPP is obtained by adding daytime respiration to A_{dt} and summing over the year.

Autotrophic respiration Maintenance respiration is calculated daily based on tissue-specific C:N ratios (cn), temperature (either air, T, or soil temperatures, T_{soil} (see Appendix Section), for above and below ground tissues, respectively), tissue biomass and phenology following the approach of Ryan (1991) and Sprugel *et al*. (1995):

$$R_{leaf} = r \cdot \frac{C_{leaf}}{cn_{leaf}} \phi \cdot g(T)$$
$$R_{sapwood} = r \cdot \frac{C_{sapwood}}{cn_{sapwood}} g(T)$$
$$R_{root} = r \cdot \frac{C_{root}}{cn_{fineroot}} \phi \cdot g(T_{soil}) \quad (22)$$

where

$$g(T) = \exp\left[308.56 \cdot \left(\frac{1}{56.02} - \frac{1}{(T + 46.02)}\right)\right] \quad (23)$$

Equation (23) is a modified Arrhenius equation (Lloyd & Taylor, 1994), where T is the temperature (°C). The use of such a relationship in preference to a fixed Q_{10} is justified by evidence for a consistent decline in the apparent Q_{10} of autotrophic respiration with temperature (Tjoelker *et al*., 1999). The PFT-specific parameter r is the respiration rate ($g\,C\,g\,N^{-1}\,day^{-1}$) on a 10 °C base. Chosen values of r crudely account for the observation that plants from warmer environments typically have much lower respiration rates at any given temperature than plants from cooler environments (Fukai & Silsburg, 1977; Lechowicz *et al*., 1980; Amthor, 1989; Ryan, 1991). Daily tissue maintenance respiration rates are summed over tissues and days to give the annual maintenance respiration for the average individual of each PFT. Multiplying by the population density gives the PFTs total maintenance respiration over the grid cell:

$$R_m = \left\{\sum_{d=1}^{365} \left(R_{leaf} + R_{sapwood} + R_{root}\right)\right\} \cdot P \quad (24)$$

After maintenance respiration is subtracted from GPP, 25% of the remainder is taken as growth respiration, the cost of producing new tissues, leaving the annual net primary productivity ($g\,C\,m^{-2}\,yr^{-1}$) (Ryan, 1991) as

$$NPP = 0.75(GPP - R_m) \quad (25)$$

Average individual growth

Tissue turnover Each living tissue is assigned a PFT-specific tissue turnover rate (Table 1) (Schoettle & Fahey, 1994), which is transferred either into litter (leaf and fine root), or from living sapwood to heartwood. Thus,

$$\Delta C_{L,ag} = \sum_{PFT} (C_{leaf}\, f_{leaf}\, P)$$
$$\Delta C_{L,bg} = \sum_{PFT} (C_{root}\, f_{root}\, P)$$
$$C_{leaf,new} = C_{leaf,old}(1 - f_{leaf}) \quad (26)$$

$$C_{sapwood,new} = C_{sapwood,old}\left(1 - f_{sapwood}\right)$$
$$C_{heartwood,new} = C_{heartwood,old} + C_{sapwood,old}\, f_{sapwood}$$
$$C_{root,new} = C_{root,old}(1 - f_{root}) \quad (27)$$

where $C_{L,ag}$ and $C_{L,bg}$ are this year's updated above- and below-ground litter, respectively.

Reproduction Reproduction costs – carbohydrate allocated to produce reproductive organs and propagules – range between 5% and 20% of NPP (Harper, 1977; Larcher, 1983). As a simple approximation, a fixed 10% fraction of annual NPP is deducted to account for allocation to reproduction. Only a minute part of this carbon enters the next generation, so in order to maintain a closed carbon cycle all of the reproductive allocation is assumed to enter the above-ground litter pool.

Allocation Once reproduction costs have been accounted for, the remaining fraction of annual NPP, the biomass increment (ΔC), is allocated to the tissue pools in such a way as to satisfy the four scaling rules (Eqns 1–4), governing plant physiognomy. Thus,

$$\Delta C = \Delta C_{leaf} + \Delta C_{sapwood} + \Delta C_{root} \quad (28)$$

where ΔC_{leaf}, $\Delta C_{sapwood}$ and ΔC_{root} represent the biomass allocation to the respective pools. Equations (1–4) and (28) are combined and the individual allocation terms derived using standard numerical methods. In years of stress, the biomass increment may not allow sufficient allocation to the leaves to fully utilize the current sapwood (given the constraint implied by Eqn. 1). This year's production is then allocated to leaves and roots only, and the excess sapwood mass transferred to the nonliving heartwood pool. In a year with severe drought there may be insufficient biomass increment to maintain both current sapwood mass and leaf mass. In this case all of the biomass increment is allocated to fine roots and excess sapwood and leaf mass transferred to the heartwood and above-ground litter pools, respectively.

For herbaceous plants, which lack wood, the biomass increment is distributed among leaves and fine roots according to Eqn. (2). Relocation of carbon is allowed from the fine roots to leaves, i.e., we assume the existence of below-ground carbon reserves, which can be mobilized in times of stress.

Vegetation structure (in terms of crown area and FPC) is updated after allocation of the biomass increment, in accordance with Eqns (1–4), (7) and (8).

Mortality

Mortality is imposed as a reduction in population density at the end of each simulation year. Mortality may occur as a result of light competition ($\mathrm{mort_{shade}}$), low growth efficiency ($\mathrm{mort_{greff}}$), a negative annual carbon balance ($\mathrm{mort_{NPP}}$), heat stress ($\mathrm{mort_{heat}}$), or when PFT bioclimatic limits are exceeded for an extended period ($\mathrm{mort_{lim}}$). The overall mortality rate for a population is the sum of the rates for individual mortality components (maximum 1), i.e.,

$$\mathrm{mort} = \max\left(\mathrm{mort_{shade}} + \mathrm{mort_{greff}} + \mathrm{mort_{NPP}} + \mathrm{mort_{heat}} + \mathrm{mort_{lim}}, 1\right) \tag{29}$$

The living biomass and heartwood of killed individuals is transferred to the above- and below-ground litter pools, i.e.,

$$\begin{aligned} P_{\mathrm{new}} &= P_{\mathrm{old}}(1 - \mathrm{mort}) \\ C_{\mathrm{L,ag,new}} &= C_{\mathrm{L,ag,old}} + P_{\mathrm{old}} \cdot \mathrm{mort} \cdot \\ &\quad \left(C_{\mathrm{leaf}} + C_{\mathrm{sapwood}} + C_{\mathrm{heartwood}}\right) \\ C_{\mathrm{L,bg,new}} &= C_{\mathrm{L,bg,old}} + P_{\mathrm{old}} \cdot \mathrm{mort} \cdot C_{\mathrm{root}} \end{aligned} \tag{30}$$

Competition for light among neighbouring individuals occurs whenever increased biomass results in a grid cell FPC of more than 1, when summed across all PFTs, or more than 0.95, when summed across woody PFTs. Mortality is imposed such that summed woody FPC is reduced to 0.95, and/or total grid cell FPC is reduced to 1. Herbaceous plants are assumed to be inferior to woody plants in competition for light, and can occupy, at most, that proportion of the grid cell (1–$\mathrm{FPC_{woody}}$) not occupied by woody plants. Shading mortality is partitioned among woody PFTs in proportion to the FPC increment resulting from their biomass increment for this year. The same rule is applied for herbaceous plants. Background mortality is calculated from this year's growth efficiency (Waring, 1983; Waring & Schlesinger, 1985), the ratio of this year's net biomass increment to leaf area:

$$\mathrm{greff} = \frac{\Delta C}{C_{\mathrm{leaf}}\mathrm{SLA}} \tag{31}$$

Following Prentice *et al*. (1993), the mortality rate is inversely related to growth efficiency:

$$\mathrm{mort_{greff}} = \frac{k_{\mathrm{mort1}}}{1 + k_{\mathrm{mort2}} \cdot \mathrm{greff}} \tag{32}$$

where k_{mort1} represents the asymptotic maximum mortality rate, and k_{mort2} is a parameter governing the slope of the relationship between mortality and growth efficiency (see Table 3). All individuals in a PFT population are killed if NPP becomes negative in any year:

$$\mathrm{mort_{NPP}} = \begin{cases} 1; & \mathrm{NPP} < 0 \\ 0; & \mathrm{NPP} \geq 0 \end{cases} \tag{33}$$

During prolonged periods with high temperatures, some plants, especially those found in temperate and boreal ecosystems, can become stressed and suffer tissue damage. Heat stress could lead to forest dieback, as has been shown under climate warming scenarios (Joos *et al*., 2001). The formulation of heat damage mortality is based on the annual accumulated degree-day sum above a PFT-specific temperature base, $T_{\mathrm{mort,min}}$ (Table 1), with mortality increasing linearly and reaching unity (complete mortality) at or above 300 degree-days above the threshold value:

$$\mathrm{mort_{heat}} = \max\left[1, \frac{\sum_{\mathrm{d}} \max\left(T_{\mathrm{d}} - T_{\mathrm{mort,min}}, 0\right)}{300}\right] \tag{34}$$

If 20-year mean values of bioclimatic variables fall outside a PFTs limits for survival (Table 2), its entire population is killed ($\mathrm{mort_{lim}} = 1$).

Disturbance regime Fire is the most important natural disturbance at a global scale, and is the only form of disturbance explicitly represented in LPJ. A full description of the fire module is given by Thonicke *et al*. (2001).

Several simplifying assumptions are made. First, fire occurrence is taken to be dependent only upon fuel load (i.e. the amount of dry combustible material, $C_{\mathrm{L,ag}}$) and litter moisture. Fire spread is not possible below a minimum fuel load, $\mathrm{fuel_{min}}$ (Table 3). Ignition sources are assumed to be available whenever fire is possible. Second, fire effects are assumed to be determined only by the length of the fire season and PFT specific 'resistances' (r_{fire}, Table 1).

A threshold value of fuel moisture content is defined as the value above which a fire would not spread. An exponential function is used to approximate the probability of the occurrence of at least one fire in a day:

$$p\left(W_{\mathrm{l,d}}\right) = \exp\left[-\pi\left(\frac{W_{\mathrm{l,d}}}{m_{\mathrm{e}}}\right)^2\right] \tag{35}$$

where $W_{l,d}$ is the daily moisture status in the upper soil layer, used here as a surrogate for litter moisture, and m_e is a PFT weighted threshold value (Table 3). The length of the fire season (in years) is taken as:

$$s = \sum_{d=1}^{365} \frac{p(W_{l,d})}{365} \quad (36)$$

A constant, nonlinear relationship between length of fire season and annual area burnt is assumed.

$$A(s) = s \cdot \exp\left[\frac{s-1}{0.45(s-1)^3 + 2.83(s-1)^2 + 2.96(s-1) + 1.04}\right] \quad (37)$$

The fraction of individuals killed within the burnt areas depends on the prescribed PFT fire resistance. Tropical raingreen and temperate broadleaved evergreen woody PFTs are relatively resistant to fire, reflecting widespread adaptations to fire among plants of dry subtropical and tropical environments. The other woody PFTs have lower resistance (Table 1). Herbaceous plants are assumed to complete their life cycle ahead of the fire season and are therefore unaffected by fire disturbance in the model.

The living biomass and heartwood of individuals killed by fire are assumed to be fully consumed, and released to the atmosphere as CO_2. Above-ground litter in the burnt fraction of a grid cell is likewise fully consumed and released as CO_2.

Establishment

Each year, new woody PFT individuals and herbaceous PFTs are established, available space permitting. Woody PFTs are subject to a maximum establishment rate of 0.24 saplings m^{-2} (Prentice *et al.*, 1993). Woody PFT saplings can establish in the proportion of the grid cell not currently occupied by woody PFTs, representing the illuminated understorey, or open ground; shading reduces establishment as summed woody FPC approaches its limit of 1. Woody PFTs within their bioclimatic limits for establishment have the same establishment rate given by:

$$\text{est} = \frac{\text{est}_{\max}\left[1 - e^{-5(1-\text{FPC}_{\text{woody}})}\right] \cdot (1 - \text{FPC}_{\text{woody}})}{n_{\text{est, woody}}} \quad (38)$$

where $n_{\text{est, woody}}$ and $\text{FPC}_{\text{woody}}$ are the number and summed FPC of woody PFTs within their bioclimatic limits for establishment (Table 2). The establishment rate increments population density:

$$P_{\text{new}} = P_{\text{old}} + \text{est} \quad (39)$$

while tissue biomass for the PFT average individual is modified to account for the addition of saplings (of prescribed biomass) to the PFT population; for each tissue (leaf, sapwood, heartwood, fine root):

$$C_{\text{tissue, new}} = \frac{C_{\text{tissue, old}} \cdot P_{\text{old}} + C_{\text{tissue, sapling}} \cdot \text{est}}{P_{\text{new}}} \quad (40)$$

Saplings are assumed to have an initial individual LAI of 1.5, from which initial biomass in each tissue is derived (by Eqns 1–4). Herbaceous PFTs can establish in nonvegetated area (not yet occupied by any PFT). The establishment rate for each herbaceous PFT is given by:

$$\text{est} = \frac{(1 - \text{FPC}_{\text{total}})}{n_{\text{est, herb}}} \quad (41)$$

where $\text{FPC}_{\text{total}}$ is the summed FPC of all PFTs (woody and herbaceous); $n_{\text{est, herb}}$ is the number of herbaceous PFTs within their bioclimatic limits for establishment. The herbaceous establishment rate modifies leaf and root biomass:

$$\begin{aligned} C_{\text{leaf, new}} &= C_{\text{leaf, old}} + C_{\text{leaf, est}} \cdot \text{est} \\ C_{\text{root, new}} &= C_{\text{root, old}} + C_{\text{root, est}} \cdot \text{est} \end{aligned} \quad (42)$$

where $C_{\text{leaf, est}}$ and $C_{\text{root, est}}$ are prescribed incremental leaf and fine root biomass values based on an LAI of 0.001.

Establishment of both woody and herbaceous PFTs is inhibited under extreme heat or water stress. A minimum annual precipitation limit ($\text{prec}_{\min}$) of 100 mm is set, below which seedlings will not germinate and so no establishment will occur. Development of seedlings and saplings is not explicitly modelled through the course of the year. The additional uptake of carbon associated with sapling establishment is therefore simply added to the annual NPP. A major simplification arising from the average-individual approach is that only one age-height class for each woody PFT is explicitly defined for a grid cell at any particular time. By updating the status of the PFT average individual, sapling properties are merged with the extant average individual properties, effectively surpassing life cycle stages, which might significantly influence the dynamics of real vegetation. This represents a major simplification in the treatment of population dynamics in the model. However, subdivision of PFTs into age-height classes is technically possible within the design of LPJ and would be important, e.g., for modelling the effects of forest management.

Soil and litter biogeochemistry

Each PFT has an associated above- and below-ground litter pool. As litter decomposes a fraction, representing the highly labile fraction, is respired as CO_2 directly into the atmosphere. The remainder is divided between the intermediate and slow SOM pools (Foley, 1995). The litter pool is assigned a decomposition rate at 10 °C of $0.35\,\text{yr}^{-1}$ while the intermediate and slow SOM pools are assigned decomposition rates at 10 °C of 0.03 and $0.001\,\text{yr}^{-1}$. These rates correspond to turnover times

(τ_{10}) of 2.86, 33.3, 1000 years, respectively (Meentemeyer, 1978; Foley, 1995).

Decomposition is soil temperature- and moisture-dependent. Temperature dependence follows the modified Arrhenius relationship (Lloyd & Taylor, 1994) also used for modelling maintenance respiration in LPJ (Eqn. 23). Above-ground litter decomposition is made dependent on air temperature, whereas below-ground litter and SOM decomposition are related to soil temperature. An empirical soil moisture relationship from Foley (1995) is adopted:

$$f(W_1) = 0.25 + 0.75 \times W_1 \tag{43}$$

where W_1 is the average moisture status in the upper soil layer in a given month. Monthly decomposition rates as a function of monthly temperature and moisture status are given by:

$$k = \frac{(1/\tau_{10})\, g(T)\, f(W_1)}{12} \tag{44}$$

Decomposition follows first-order kinetics (Olson, 1963):

$$\frac{\mathrm{d}C}{\mathrm{d}t} = -kC \tag{45}$$

where C is the pool size, t is time and k the monthly decomposition rate. Integrating with respect to time t,

$$C = C_0 \cdot e^{-kt} \tag{46}$$

gives C, the pool size at any time t, with C_0 representing its initial size. The amount of carbon decomposed in one month is,

$$C_0\left(1 - e^{-k}\right) \tag{47}$$

Following Foley (1995), 70% of the decomposed litter goes directly into the atmosphere as CO_2 (f_{air}), the remaining 30% entering the soil pools, with 98.5% (f_{inter}) and 1.5% (f_{slow}) of the remainder entering the intermediate and slow soil pools, respectively. Summation of the monthly litter and soil decomposition terms gives total monthly heterotrophic respiration, R_{h}:

$$R_{\mathrm{h}} = \Phi_{\mathrm{litter}} + \Phi_{\mathrm{inter}} + \Phi_{\mathrm{slow}} \tag{48}$$

where Φ_{litter}, Φ_{inter} and Φ_{slow} are carbon emissions from the litter pools, the intermediate and slow soil pools, respectively.

Input data

Monthly fields of mean temperature, precipitation and cloud cover were taken from the CRU05 (1901–1998) monthly climate data on a $0.5^\circ \times 0.5^\circ$ global grid, provided by the Climate Research Unit (CRU), University of East Anglia (New *et al*., 1999a, b, unpublished). Cloud cover data for 1997 and 1998, not so far compiled by CRU, were taken as the average over the previous 30 years. Monthly data were interpolated to provide 'quasi-daily' time series of climate. A data set of historical global atmospheric CO_2 concentrations extending from 1901 to 1995 was obtained courtesy of the Carbon Cycle Model Linkage Project (Kicklighter *et al*., 1999; McGuire *et al*., 2001). These data were derived from a combination of ice-core measurements (Etheridge *et al*., 1996) and atmospheric observations (Keeling *et al*., 1995). The dataset was extended to 1998 using the same procedure. Soil texture data were as in BIOME3 (Haxeltine & Prentice, 1996a), based on the FAO soil data set (Zobler, 1986; FAO, 1991).

From remote sensing (Advanced Very High Resolution Radiometer, AVHRR), Defries *et al*. (2000) generated a global map at 1 km spatial resolution of percentage tree cover, and maps partitioning the woody vegetation according to phenology (evergreen vs. deciduous) and leaf morphology (broadleaf vs. needleleaf) [http://glcf.umiacs.umd.edu]. These data were aggregated to a $0.5^\circ \times 0.5^\circ$ grid for comparison with LPJ simulation results. Observations of atmospheric CO_2 concentrations from a network of 27 monitoring stations were obtained from a programme of the National Oceanographic and Atmospheric Administration (NOAA) (GLOBALVIEW-CO_2, 1999). The monthly station records were post-processed to extract the detrended, average monthly observations between 1983 and 1992 (Heimann *et al*., 1998). This same procedure was applied to model outputs before the net monthly fluxes were passed to the atmospheric tracer transport model, TM2. Monthly fluxes of CO_2 between the atmosphere and the ocean surface were obtained from a standard run of the Hamburg Model of the Ocean Carbon Cycle (HAMOCC3, see Maier-Reimer, 1993) including a NPZD-type marine biosphere model (Kurz, 1993; Six & Maier-Reimer, 1996). Monthly CO_2 emissions fields from fossil-fuel burning and cement manufacture were computed based on a global $1^\circ \times 1^\circ$ map compiled by Marland *et al*. (1989), assuming constant emissions throughout the year (Heimann *et al*., 1998). Reduced-form 'station matrices' (see Kaminski *et al*., 1999a, b) were derived from the TM2 atmospheric tracer transport model (Heimann *et al*., 1989) using wind fields based on the 12-h analyses of the European Centre for Medium-Range Weather Forecasts for the year 1987. A global $1^\circ \times 1^\circ$ data set of annual runoff was used (Cogley, 1991). Measurements of meteorological data (temperature, precipitation and net incoming solar radiation), and fluxes of net ecosystem exchange, NEE, for six EUROFLUX sites were obtained courtesy of the EUROFLUX monitoring network [http://www.unitus.it/dipartimenti/disafri/progetti/eflux/euro.html]. Data for the soil moisture balance evaluation were provided by the Global Soil Moisture Data Bank [http://metosrv2.umd.edu/~alan/soil_moisture/rus

wet. forcing.6sta.readme.html] (Robock *et al*., 1995) and Goutorbe *et al*. (1989); Goutorbe & Tarrieu (1991); Cammeraat & Prinsen (1995); Cammeraat (1996) and Menzel (1997).

Modelling protocol

A typical simulation with LPJ starts from 'bare ground' (no plant biomass present) and 'spins up' for 1000 model years until approximate equilibrium is reached with respect to carbon pools and vegetation cover. It is appropriate to drive the model with an approximately constant climate during the spin up phase; however, since fires in many regions occur only in drier years, repeating a single year's climate or even using a long-term climatic average, can lead to anomalous results. The spin-up therefore requires the use of an interannually varying climate, with annual-average temperatures, precipitation and cloudiness fluctuation about constant long-term means. In order to enhance computational efficiency, the size of the slow SOM pool is solved analytically after 400 years. The spin-up is continued for a further 600 years to ensure closeness to equilibrium in the slower carbon pools. The model can then be driven with a transient climate.

In a standard simulation LPJ is run in the transient phase using the CRU data for 1901–1998. For the comparison against the EUROFLUX site climate data, the available monthly site data were first regressed against the corresponding CRU data, for the nearest grid cell, and then historical 1901–1998 site climatologies were constructed. For seasonal soil moisture-balance analysis, the site climate data were used directly.

To simulate seasonal cycles of atmospheric CO_2 at the regional scale, monthly net carbon exchanges for each $0.5^\circ \times 0.5^\circ$ grid cell over the globe were calculated from LPJ-predicted heterotrophic respiration, biomass burnt and NPP, i.e.,

$$\mathrm{NEE} = R_\mathrm{h} + \mathrm{BiomassBurning} - \mathrm{NPP} \qquad (49)$$

Detrended averages of NEE for 1982–1993 were derived as in Heimann *et al*. (1998) and used as input to an atmospheric transport model (Heimann *et al*., 1989), whose outputs were 'sampled' at the locations of the measuring stations.

Results

Local scale (site, stand, 1 km^2)

Vegetation dynamics Successional dynamics from an initially unvegetated state are illustrated for a selection of 'sites' representing boreal, temperate and tropical forests, a tropical savanna and a temperate grassland (Fig. 2). All these sites show an initial high abundance of herbaceous plants, attained within a few years. At the tropical rainforest site year-round favourable conditions for tree growth enable the Tropical Evergreen PFT to rapidly achieve dominance over the herbs. Raingreen (tropical deciduous) trees never become abundant because they are outcompeted by evergreens. At the temperate forest site, a diverse mixture of temperate tree types comes more slowly (over c. 40 years) to shade out the herbaceous plants. In the boreal forests with cold winter temperatures and a short growing season, only cold-tolerant woody PFTs survive. The model correctly simulates the mixture of evergreen needle-leaved and deciduous broad-leaved woody PFTs dominating over herbaceous plants from c. 50 years. Note that since age-class structure is not explicitly modelled, the observed decline in stand productivity of mature forests (Yoder *et al*., 1994; Landsberg & Gower, 1997; Ryan *et al*., 1997) is not simulated by LPJ.

In water-limited ecosystems, the herbaceous vegetation (normally grasses) may grow rapidly enough to greatly deplete soil water in the upper soil layer, inhibiting the growth of trees, which have a greater fraction of their roots in the lower soil layers. In addition, fire is a constant feature of many semiarid ecosystems and tends to favour grasses over trees. These features are captured correctly in the simulated dynamics of the savanna and grassland sites. In the savanna, a fluctuating mixture of woody PFTs (most importantly, tropical raingreen broad-leaved trees) coexists with a herbaceous cover. In the grassland, herbaceous plants maintain overwhelming dominance.

Seasonal carbon exchange Figure 3 shows the modelled and measured monthly net fluxes of CO_2 (NEE) at six flux monitoring sites from the EUROFLUX campaign. All sites are forests comprising various combinations of boreal, temperate and mediterranean PFTs. Simulated results of monthly NEE show reasonable agreement with observation. The amplitude of the growing-season NEE and the phase are generally successfully reproduced.

Seasonal water balance Soil-moisture data from various sources and locations including boreal, temperate and mediterranean climates were compared with LPJ estimates (Fig. 4). Site measurements of parameters such as soil texture, water holding capacities, percolation rate, vegetation structure and albedo were used to drive the model, when available. LPJ tended to slightly overestimate soil moisture levels during the early growing season at the Russian sites, but otherwise showed good agreement over the whole seasonal cycle across all environments.

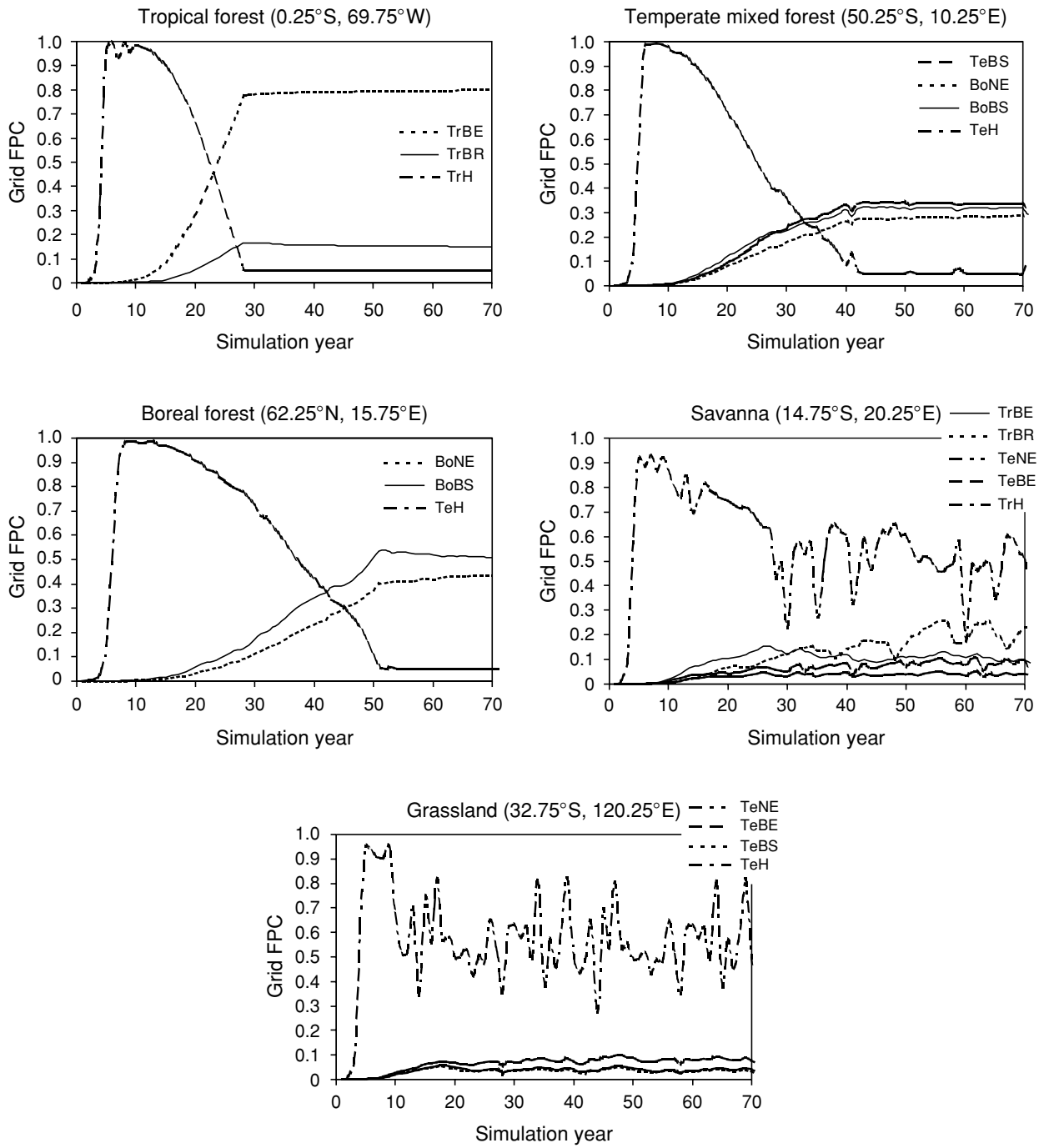

Fig. 2 Simulated successional dynamics in different environments. Changes in relative FPC (fractional cover) of different plant functional types (PFTs) during the initial years of simulation from 'bare ground', PFT abbreviations given in Table 1.

Regional scale (latitude bands, continents)

Seasonal cycle of atmospheric CO_2 Terrestrial ecosystem functioning causes a strong northward increase in the amplitude of the seasonal cycle of CO_2 concentration in the atmosphere (Fung *et al.*, 1983; Heimann *et al.*, 1998; Prentice *et al.*, 2000). The differential impact of the temperature seasonality on production and respiration over the extensive northern land mass results in a pronounced oscillation of spatially integrated NEE. Advection to the high latitudes causes a seasonal range of 15 ppm or more in CO_2 concentrations measured at Arctic stations. CO_2 concentrations measured in the tropics are influenced both by air transported from the

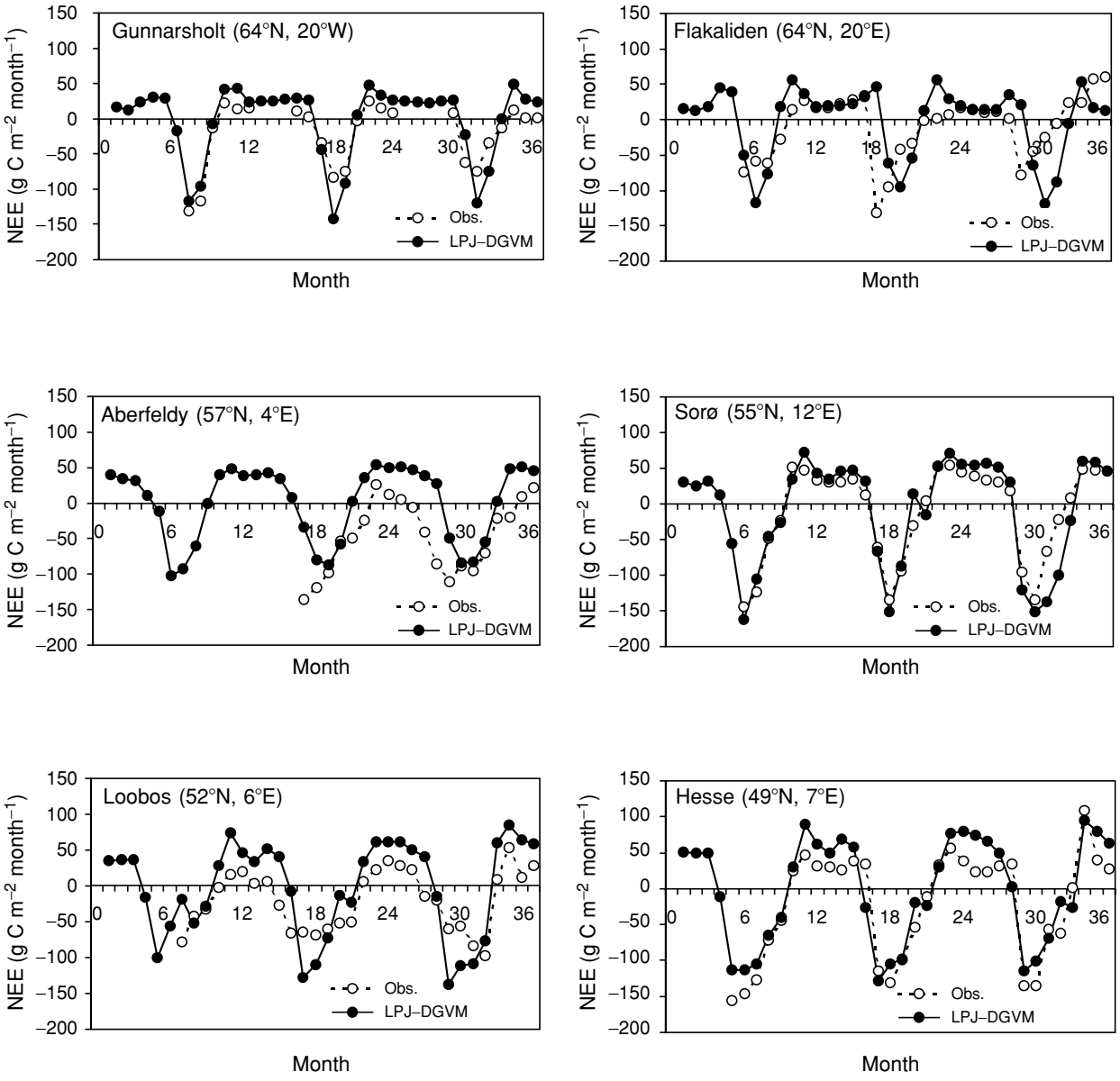

Fig. 3 Observed vs. simulated monthly fields of Net Ecosystem Exchange (NEE, g C m^{-2}; here and elsewhere positive values represent a flux to the atmosphere; negative values a flux to the biosphere), at six EUROFLUX sites.

north, and by the response of tropical ecosystems to seasonality in precipitation (Heimann *et al*., 1998). The relative contribution of the oceans to the seasonal cycle increases in the south where there is relatively little land. LPJ was able to capture the observed seasonal cycle convincingly at all 27 stations, and compared favourably with the other terrestrial biosphere models in Heimann *et al*. (1998). Figure 5 illustrates these results for a representative subset of stations. At the 12 stations north of 30°N, LPJ is slightly out of phase (1 week) with observations, simulating an early drawdown of CO_2, and slightly over-estimates the amplitude of the summer CO_2 drawdown. LPJ simulates correctly the phase of the seasonal cycle at the nine tropical stations but the amplitudes are somewhat under-estimated. At the six remaining stations (latitudes south of 30°S), LPJ generally fits both the phase and the amplitude of the cycle.

Global scale

Vegetation structure (comparison with satellite data) Three global maps (Fig. 6) summarize the potential natural vegetation simulated by LPJ for the modern climate. The model realistically predicts the dominant PFT

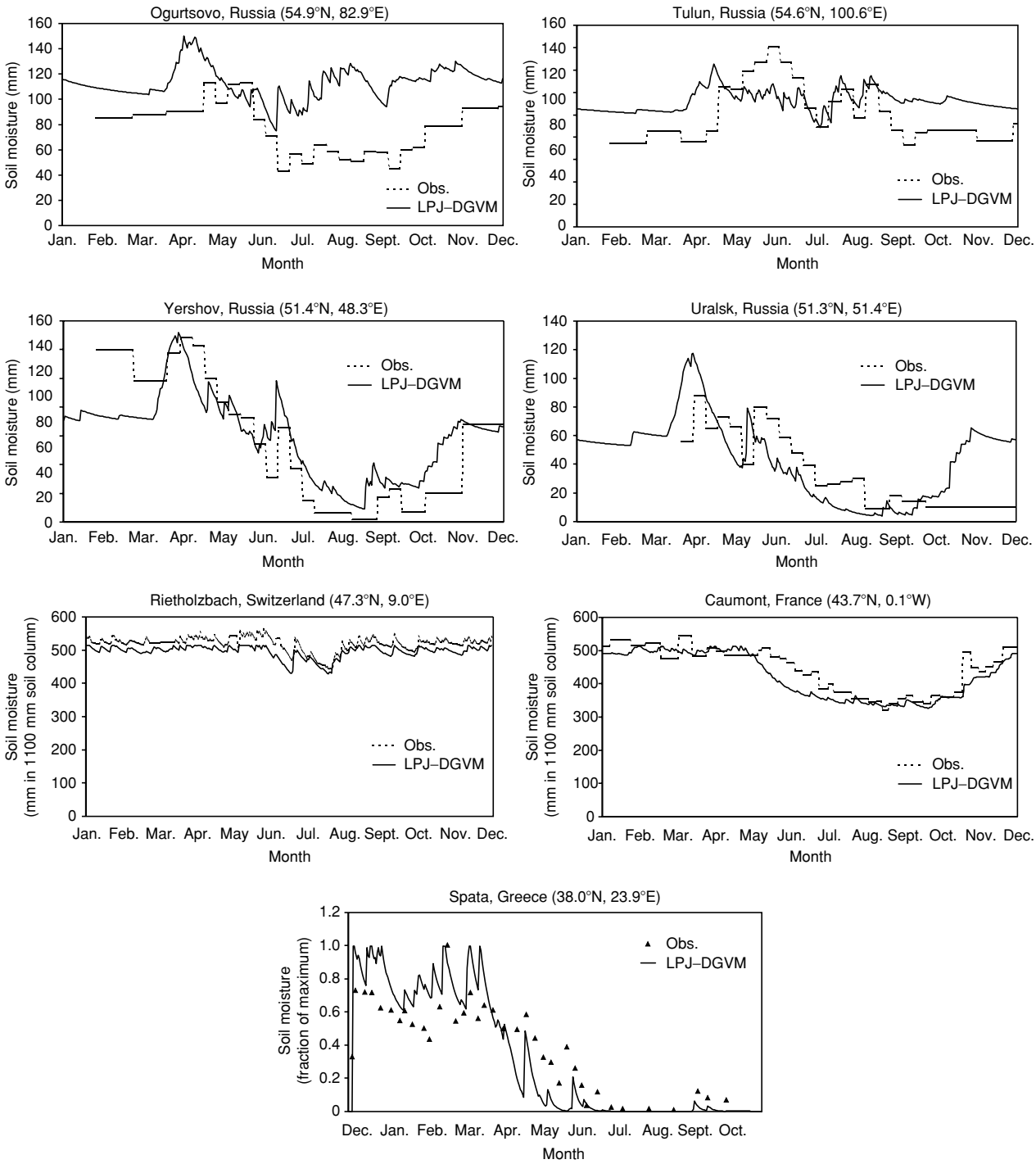

Fig. 4 Observed vs. simulated seasonal soil moisture at seven sites.

(i.e. with highest simulated areal cover) in most regions (Fig. 6). The large area of boreal evergreen forest in Canada and northern Eurasia, the boreal deciduous forests in Siberia, and the transition into temperate ecosystems of north America, western Europe and China are clearly represented. Further south, LPJ simulates the transition from drought-deciduous forests or savanna of the wet–dry subtropics into evergreen rainforests in wet climates near the equator. LPJ is also reasonably successful in simulating nonwooded areas, including grasslands,

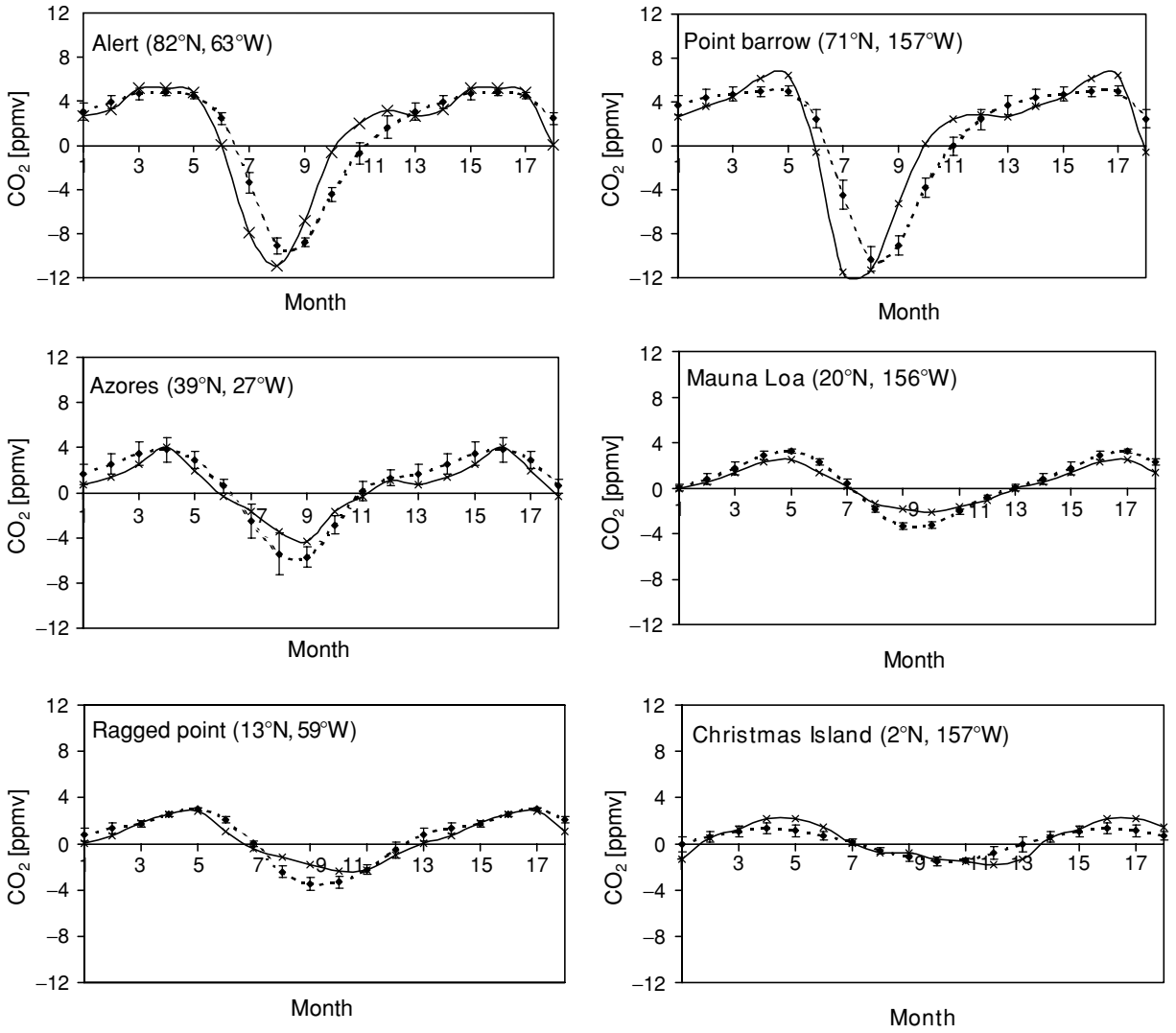

Fig. 5 Observed (dotted line, showing mean and standard deviation) vs. simulated (solid line) seasonal cycle of CO_2 at six monitoring stations. Observations are from the NOAA data set (Conway *et al.*, 1994).

but tends to overestimate the woody component (e.g. in the African sahel and in the North American prairie). LPJ simulates northern tundra, and grasslands in dry areas including the western USA, parts of southern Europe, central Asia and interior Australia.

Figure 6 also shows the fractional coverage of vegetation types partitioned according to phenology class (evergreen woody, deciduous woody, herbaceous), and leaf morphology (broadleaf herbaceous, needleleaf woody and herbaceous), respectively. Compared to a satellite-derived data set (Fig. 7), LPJ over-predicts the coverage of deciduous broadleaved vegetation in the boreal forests of Canada and Eurasia, but the general pattern – with maximum needleleaf evergreen dominance in the 'core' area falling off to the north and south – is shown correctly. Comparison of simulated and satellite-derived leaf phenology and leaf type also confirms that the transition along precipitation gradients in the tropics and subtropics – from desert, through broad-leaved deciduous forests or savannas to broadleaved evergreen forests – are represented reasonably well by LPJ.

Global runoff LPJ-simulated estimates of daily runoff were summed over the year and the annual totals averaged over 1980–1998, giving a global total of $35.4 \times 10^{12}\,m^3\,yr^{-1}$. Estimates for the global total range from $36.5 \times 10^{12}\,m^3\,yr^{-1}$ (Chanine, 1992) to $45.5 \times 10^{12}\,m^3\,yr^{-1}$ (Cogley, 1991). The zonal distribution of average runoff predicted by the model also compares favourably to a $1^\circ \times 1^\circ$ gridded data set of observed runoff (Fig. 8) (Cogley, 1991; Sitch, 2000).

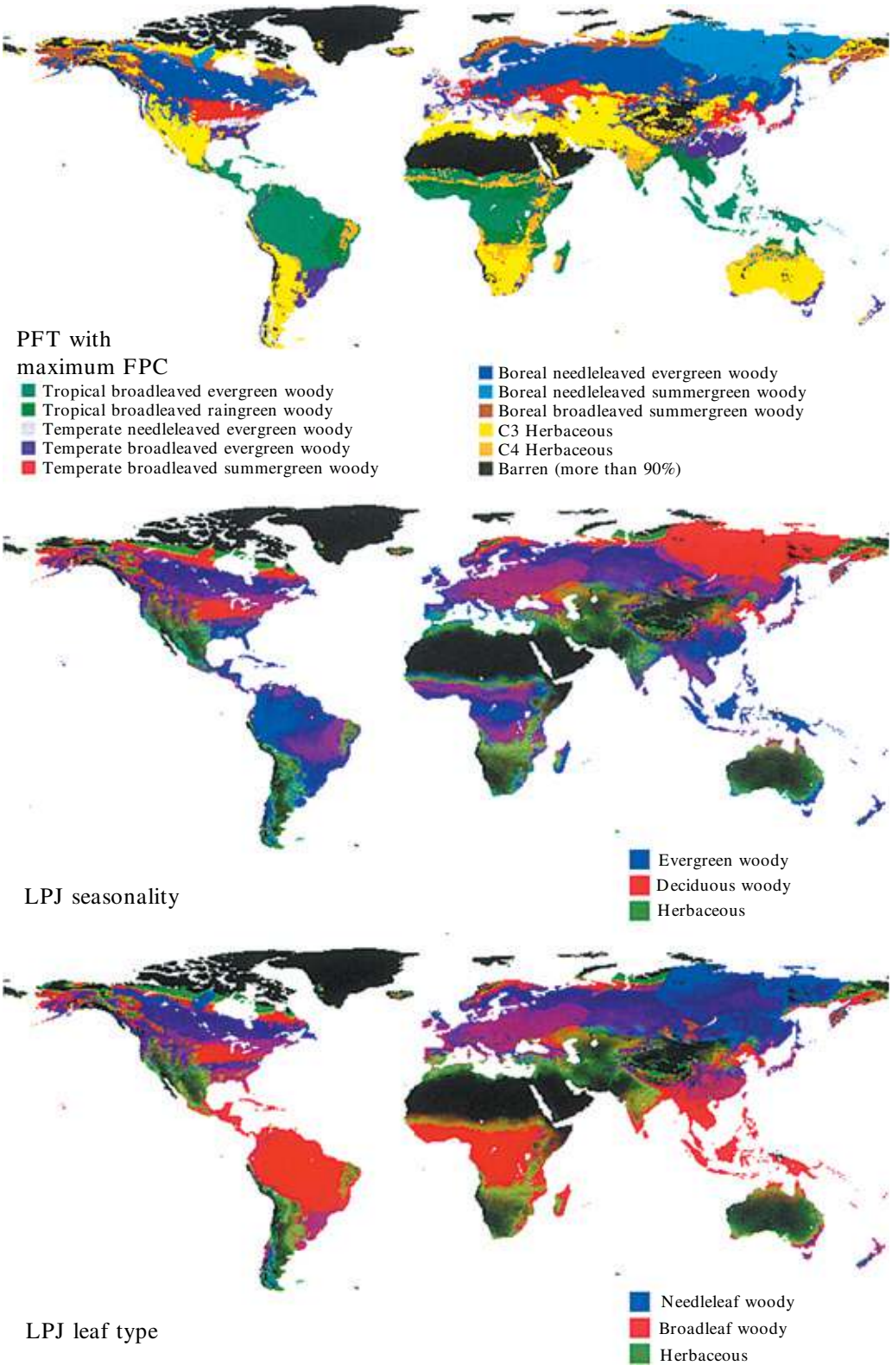

Fig. 6 LPJ-simulated dominant PFT (upper) Red–Green–Blue composite-colour (RGB) map of simulated vegetation partitioned according to phenology (middle), i.e., evergreen woody, deciduous woody and herbaceous; RGB map of simulated vegetation morphology (lower), i.e., broadleaf woody, needleleaf woody and herbaceous.

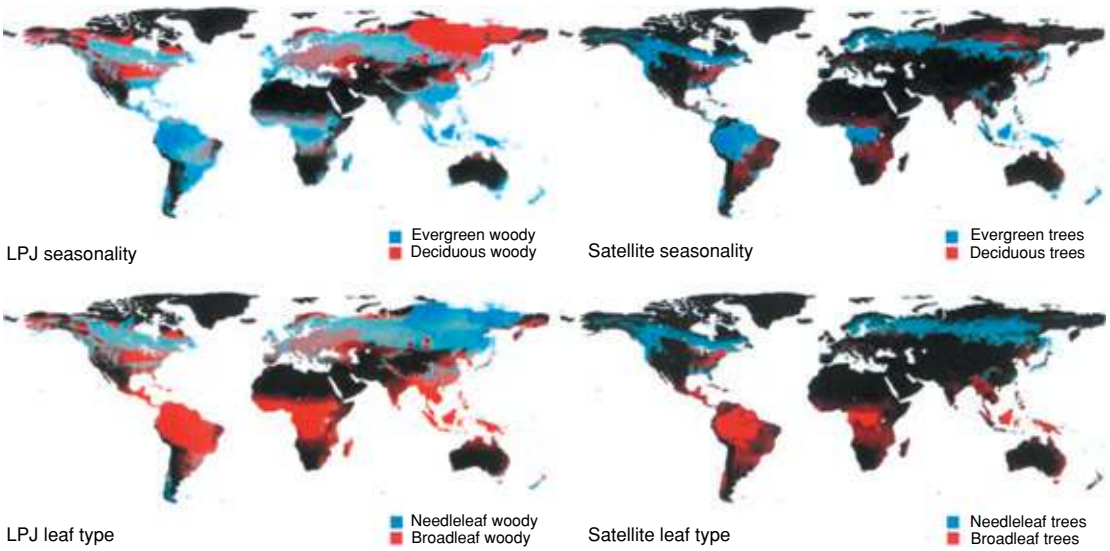

Fig. 7 Comparison of LPJ-simulated distributions of woody vegetation with satellite-based maps, for percentage tree cover, partitioned according to phenology (evergreen vs. deciduous), and leaf morphology (broadleaf vs. needleleaf).

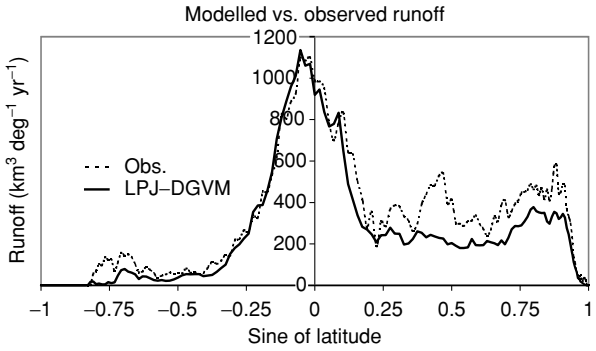

Fig. 8 Global zonal distributions of observed (Cogley, 1991) vs. simulated annual runoff.

Global carbon budgets and exchange LPJ simulated global totals for preindustrial equilibrium vegetation, soil and litter carbon are 923, 1670 and 171 Pg C, respectively. All of these estimates are within the range of other model studies (e.g. Raich *et al*., 1991; Foley *et al*., 1996; Kucharik *et al*., 1999), although vegetation carbon is at the high end of the range. Over the historical period all pools increase (simulated vegetation, soil and litter carbon for 1998 are 948, 1684 and 182 Pg C, respectively). The greatest simulated increase is in vegetation carbon, reflecting the delay between production of additional living biomass and transfer to the litter and soil pools. Global preindustrial NPP is estimated by the model to be 64 Pg C year^{-1}, increasing to an average of c. 70 Pg C year^{-1} during the 1980s. These estimates are at the higher end of the range of 44.4–66.3 Pg C year^{-1} for terrestrial biogeochemistry models included in the Potsdam NPP Intercomparison Project (Cramer *et al*., 1999). However, the majority of these predictions are based on the CLIMATE 1930–1961 average monthly climatology (an update on Leemans & Cramer, 1991) and an atmospheric CO_2 concentration of 340 ppmv, and this may explain why LPJs prediction (which takes into account 1980s climatology and CO_2 levels) is somewhat higher. The preindustrial biomass burning flux was estimated at c. 8 Pg C year^{-1}, with interannual variability of c. $\pm$0.75 Pg C year^{-1}. Current literature estimates of the burning flux range between 2 and 5 Pg C year^{-1} (Andreae, 1991; Malingreau & Zhuang, 1998) but these numbers are not well constrained. Figures 9 and 10 show LPJ predictions of the geographical distribution of soil and vegetation carbon and NPP for the modern climate.

Increasing amplitude of the seasonal cycle of atmospheric CO_2 at Mauna Loa The simulated trend in the amplitude of the seasonal cycle of atmospheric CO_2 at the Mauna Loa monitoring station between 1960 and 1992, relative to the amplitude in 1960, is in reasonably good agreement with observations (McGuire *et al*., 2001) although the interannual variability in amplitude is somewhat overestimated. McGuire *et al*. (2001) broke down the trend predicted by LPJ into CO_2 vs. climate driven components, and found that the main trend is a consequence of the CO_2 increase, leading to enhanced summertime carbon uptake in mid-latitudes.

Interannual variability in terrestrial ecosystem exchange Figure 11 shows the modelled interannual exchange of CO_2 between the global terrestrial biosphere and the

atmosphere for the period 1958–1998. The model results are compared against a 'reconstructed' net exchange calculated from the fossil fuel emission flux (Marland *et al*., 1989), the measured annual increase in atmospheric CO_2 concentration and a model-based estimate of long-term average ocean uptake (Heimann, 1997; Prentice *et al*., 2000). The effects of land use changes are not included here, but are a focus of an additional study within the Carbon Cycle Model Linkage Project (CCMLP; McGuire *et al*., 2001). LPJ-simulated fluxes are in phase with the reconstructed fluxes, suggesting (a) that terrestrial processes are the major contributor to interannual variability in CO_2 uptake and (b) that the major aspects of global-scale variability in terrestrial carbon exchange are captured by LPJ. The most obvious features of the data and simulation are the outgassing of CO_2 during El Niño events (e.g. 1983, 1987) (Prentice *et al*., 2000, 2001). The anomalous uptake of CO_2 after the 1991 Pinatubo eruption is also captured by the model. The model tends to overestimate the amplitude of the ENSO related cycle; this is consistent with the existence of a significant, but smaller, oppositely phased effect in ocean-atmosphere CO_2 exchange (Prentice *et al*., 2001).

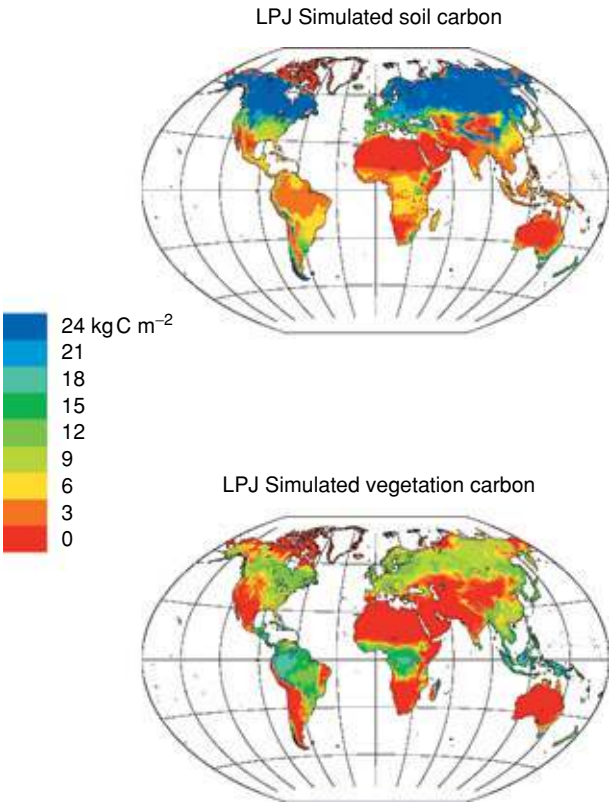

Fig. 9 LPJ-simulated global fields of vegetation and soil carbon (kg C m^{-2}) for the modern climate.

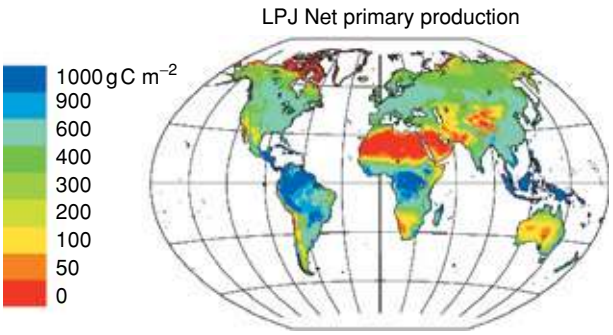

Fig. 10 LPJ-simulated global fields of NPP for the modern climate (g C m^{-2}).

Discussion

Local-scale model evaluations have shown that LPJ is able to reproduce the amplitude and phase of carbon and water exchanges with the atmosphere on the seasonal time scale. Simulated global totals and spatial distributions of soil, litter and vegetation carbon pools and annual NPP and runoff are within their accepted ranges and agree with observed patterns. LPJ estimates of global annual NPP, and hence the amount of living biomass that can be maintained, are in the generally accepted ranges of these quantities although they lie toward the upper end of current estimates. The broad-scale global vegetation distribution is in general agreement with satellite-derived maps of phenology and leaf types. The model has been evaluated with success against the detrended average seasonal cycle (as a function of latitude), the observed increase in amplitude of the seasonal cycle of atmospheric CO_2, and the interannual global exchange of CO_2 with the atmosphere. It captures key features including the aggregated response to El Niño events, and the increased uptake of atmospheric CO_2 during the years following the eruption of Mt. Pinatubo in 1991.

LPJ was one of six DGVMs that took part in the Global Change and Terrestrial Ecosystem DGVM intercomparison project (Cramer *et al*., 2001). The models were driven by the HADCM2 historical and future climate anomaly fields, with historical atmospheric CO_2 concentrations up to 1995 and the IS92a IPCC projection thereafter. LPJ results are in general agreement with the other models, projecting a continuing biosphere sink for atmospheric CO_2, peaking around 2050. Beyond this date, the modelled sink strength declines, due to progressive saturation of the CO_2 fertilization response combined with increased heterotrophic respiration in conjunction with increasing temperatures. This study also showed that simulated vegetation was far from equilibrium at 2100, emphasizing the importance of using dynamic models (DGVMs) to project changes in ecosystem composition and functioning under a rapidly changing climate.

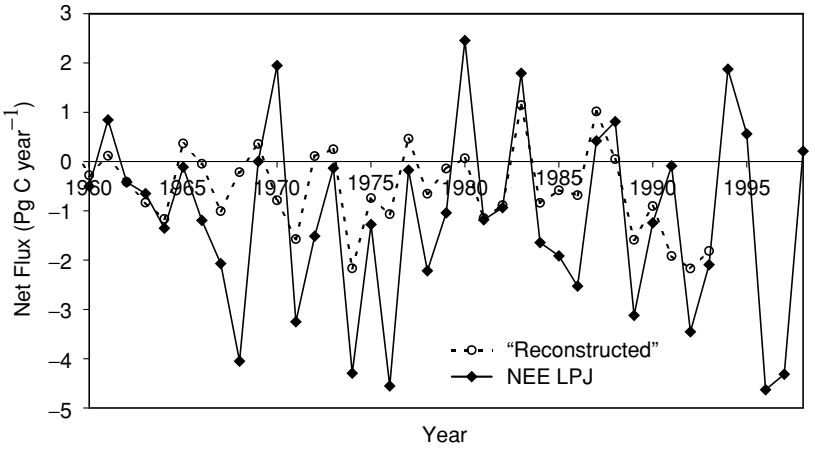

Fig. 11 Simulated vs. reconstructed interannual variation in net ecosystem exchange for the globe.

LPJ is being developed further, as a community model. The intention is to maintain a continued process of improvement driven by advances in understanding of ecological processes, ecosystem dynamics, plant physiology and the global carbon cycle. Insights gained from regional case studies will lead to model improvements and may draw attention to processes important to regional ecosystem dynamics currently not included in the model, such as permafrost at high latitudes. LPJ is also being adapted as a component of several coupled climate-carbon cycle models, and it has been incorporated in the Bern carbon cycle model, which has been used for the analysis of feedbacks in the carbon cycle under various emissions scenarios over the coming century (Joos *et al*., 2001; Prentice *et al*., 2001).

Acknowledgements

We acknowledge with thanks financial support from EPRI, USA for funding LPJ development and evaluation via the VEMAP and CCMLP projects. The CRU05 climate data were supplied by the Climate Impacts LINK Project (UK Department of the Environment Contract EPG 1/1/16) on behalf of the Climatic Research Unit, University of East Anglia. The authors wish to thank M. Heimann and T. Kaminski for providing the TM2 matrices and for their support. We also thank NOAA/INSTAAR for the GLOBALVIEW-CO_2 data and the EUROFLUX activity and Global Soil Moisture Data Bank for data used in the carbon flux and seasonal water balance analyses. L. Menzel provided the Rietholzbach hydrology data. F. Badeck and V. Brovkin commented helpfully on earlier drafts. The authors wish to thank J. Foley for a constructive review.

References

Amthor JS (1989) *Respiration and Crop Productivity*. 215 pp. Springer, New York.

Andreae MO (1991) Biomass burning: its history, use, and distribution and its impact on environmental quality and global climate. In: *Global Biomass Burning: Atmospheric, Climatic, and Biospheric Implications* (ed. Levine JS), pp. 3–21. The MIT Press, Cambridge, Massachusetts.

Berninger F, Nikinmaa E (1994) Foliage area – sapwood area relationships of Scots pine (*Pinus sylvestris*) trees in different climates. *Canadian Journal of Forest Research*, **24**, 2263–2268.

Botkin DB, Janak JK, Wallis JR (1972) Some ecological consequences of a computer model of forest growth. *Journal of Ecology*, **60**, 849–872.

Brooks A, Farquhar GD (1985) Effects of temperature on the CO_2/O_2 specificity of ribulose-1,5 bisphosphate carboxylase/oxygenase and the rate of respiration in the light. *Planta*, **165**, 397–406.

Brovkin V, Ganopolski A, Claussen M *et al. (1999) Modelling climate response to historical land cover change*. *Global Ecology and Biogeography*, **8**, 509–517.

Brovkin V, Ganopolski A, Svirezhev Y (1997) A continuous climate-vegetation classification for use in climate-biosphere studies. *Ecological Modelling*, **101**, 251–261.

Bugmann H, Cramer W (1998) Improving the behaviour of forest gap models along drought gradients. *Forest Ecology and Management*, **103**, 247–263.

Cammeraat LH (1996) The MEDALUS core field programme: An overview of sites and methodology. In: *Mediterranean Desertification and Land-Use* (eds Brandt J, Thornes JB), pp. 87–110. Wiley, Chichester.

Cammeraat LH, Prinsen HAM (1995) The MEDALUS application on CD-ROM. *Chaumont-Gistoux/Amsterdam: Da Vinci/Uva-FGBL*, **154**, 110Mb pp.

Campbell JS, Norman JM (1998) *An Introduction to Environmental Biophysics*, 286 pp. Springer.

Cao M, Woodward FI (1998) Dynamic responses of terrestrial ecosystem carbon cycling to global climate change. *Nature*, **393**, 249–252.

Chanine MT (1992) The hydrological cycle and its influence on climate. *Nature*, **359**, 373–380.

Ciais P, Denning AS, Tans PP *et al.* (1997) A three-dimensional synthesis study of $d^{18}O$ in atmospheric CO_2 1. Surface fluxes. *Journal of Geophysical Research*, **102** (D5), 5857–5872.

Cogley JG (1991) *GGHYDRO – Global Hydrographic Data Release 2.0*. Department of Geography. Trent University.

Collatz GJ, Ball JT, Grivet C *et al.* (1991) Physiological and environmental regulation of stomatal conductance, photosynthesis and transpiration: a model that includes a laminar boundary layer. *Agricultural and Forest Meteorology*, **54**, 107–136.

Collatz GJ, Ribas-Carbo M, Berry JA (1992) Coupled photosynthesis-stomatal conductance model for leaves of C_4 plants. *Australian Journal of Plant Physiology*, **19**, 519–538.

Conway TJ, Tans PP, Waterman LS (1994) Atmospheric CO_2 from sites in the NOAA/CMDL air sampling network. In: *Trends ''93: a Compendium of Data on Global Change* (eds Boden TA *et al.*), pp. 41–119. Carbon Dioxide Inf. Anal. Center. Oak Ridge National Laboratory, Oak Ridge, Tenn.

Cox PM, Betts RA, Jones CD *et al.* (2000) Acceleration of global warming due to carbon-cycle feedbacks in a coupled climate model. *Nature*, **408**, 184–187.

Cox PM, Huntingford C, Harding RJ (1998) A canopy conductance and photosynthesis model for use in a <GCM> land surface scheme. *Journal of Hydrology*, **212–213**, 79–94.

Cramer W, Bondeau A, Woodward FI (2001) Global response of terrestrial ecosystem structure and function to CO_2 and climate change: results from six dynamic global vegetation models. *Global Change Biology*, **7**, 357–373.

Cramer W, Kicklighter DW, Bondeau A *et al.* (1999) Comparing global models of terrestrial net primary productivity (NPP): overview and key results. *Global Change Biology*, **5**, 1–16.

Defries RS, Hansen MC, Townshend JRG *et al.* (2000) A new global 1-km dataset of percentage tree cover derived from remote sensing. *Global Change Biology*, **6**, 247–254.

Dewar RC (1996) The correlation between plant growth and intercepted radiation: an interpretation in terms of optimal plant nitrogen content. *Annuals of Botany*, **78** (1), 125–136.

Etheridge DM, Steele LP, Langenfelds RL *et al.* (1996) Natural and anthropogenic changes in atmospheric CO_2 over the last 1000 years from air in Antarctic ice and firn. *Journal of Geophysical Research*, **101**, 4115–4128.

FAO (1991) *The Digitized Soil Map of the World (Release 1.0)*. Vol. 67/1. Food and Agriculture Organization of the United Nations.

Farquhar GD, Lloyd J, Taylor JA *et al.* (1993) Vegetation effects on the isotope composition of oxygen in atmospheric CO_2. *Nature*, **363**, 439–442.

Farquhar GD, von Caemmerer S (1982) Modelling of photosynthetic response to environmental conditions. In: *Physiological Plant Ecology II: Water Relations and Carbon Assimilation* (eds Nobel PS, Osmond CB, Ziegler H), pp. 549–587. Springer, Berlin.

Farquhar GD, von Caemmerer S, Berry JA (1980) A biochemical model of photosynthetic CO_2 assimilation in leaves of C_3 plants. *Planta*, **149**, 78–90.

Foley JA (1995) An equilibrium model of the terrestrial carbon budget. *Tellus*, **47B**, 310–319.

Foley JA, Kutzbach JE, Coe MT *et al.* (1994) Feedbacks between climate and boreal forests during the Holocene epoch. *Nature*, **371**, 52–54.

Foley JA, Levis S, Prentice IC *et al.* (1998) Coupling dynamic models of climate and vegetation. *Global Change Biology*, **4**, 561–579.

Foley JA, Prentice IC, Ramankutty N *et al.* (1996) An integrated biosphere model of land surface processes, terrestrial carbon balance, and vegetation dynamics. *Global Biogeochemical Cycles*, **10** (4), 603–628.

Friedlingstein P, Fung I, Holland E *et al.* (1995) On the contribution of CO_2 fertilization to the missing biospheric sink. *Global Biogeochemical Cycles*, **9** (4), 541–556.

Friend AD, Stevens AK, Knox RG *et al.* (1997) A process-based terrestrial biosphere model of ecosystem dynamics (Hybrid v3.0). *Ecological Modelling*, **95**, 249–287.

Fukai S, Silsburg JH (1977) Responses of subterranean clover communities to temperature II. Effects of temperature on dark respiration rate. *Australian Journal of Plant Physiology*, **4**, 159–167.

Fulton MR, Prentice IC (1997) Edaphic controls on the boreonemoral forest mosaic. *Oikos*, **78**, 291–298.

Fung IY, Prentice K, Matthews E *et al.* (1983) Three-dimensional tracer model study of atmospheric CO_2: response to seasonal exchanges with the terrestrial biosphere. *Journal of Geophysical Research*, **88**, 1281–1294.

GLOBALVIEW-CO2 (1999) *Cooperative Atmospheric Data Integration Project – Carbon dioxide*. CD-ROM. Boulder, NOAA CMDL, Colorado.

Goutorbe JP, Noilhan J, Cuenca R *et al.* (1989) Soil moisture variations during HAPEX-MOBILHY. *Annales Geophysicae*, **7**, 415–426.

Goutorbe JP, Tarrieu C (1991) Hapex Mobilhy data base. In: *Land Surface Evaporation* (eds Schmugge TJ, André J-C), pp. 403–410. Springer, Berlin.

Harper J (1977) *Population Biology of Plants*. Academic Press, London.

Haxeltine A, Prentice IC (1996a) BIOME3: An equilibrium terrestrial biosphere model based on ecophysiological constraints, resource availability, and competition among plant functional types. *Global Biogeochemical Cycles*, **10** (4), 693–709.

Haxeltine A, Prentice IC (1996b) A general model for the light-use efficiency of primary production. *Functional Ecology*, **10**, 551–561.

Haxeltine A, Prentice IC, Cresswell ID (1996) A coupled carbon and water flux model to predict vegetation structure. *Journal of Vegetation Science*, **7** (5), 651–666.

Heimann M (1997) A review of the contemporary global carbon cycle and as seen a century ago by Arrhenius and Högbom. *Ambio*, **26** (1), 17–24.

Heimann M, Esser G, Haxeltine A *et al.* (1998) Evaluation of terrestrial carbon cycle models through simulations of the seasonal cycle of atmospheric CO_2: first results of a model intercomparison study. *Global Biogeochemical Cycles*, **12** (1), 1–24.

Heimann M, Keeling CD, Tucker CJ (1989) A three-dimensional model of atmospheric CO_2 transport based on observed winds, part 3. Seasonal cycle and synoptic time scale variations. *Geophysical Monographs*, **55**, 277–284.

Huang S, Titus SJ, Wiens DP (1992) Comparison of nonlinear height-diameter functions for major Alberta tree species. *Canadian Journal of Forest Research*, **22**, 1297–1304.

Jackson RB, Canadell J, Ehleringer JR *et al.* (1996) A global analysis of root distributions for terrestrial biomes. *Oecologia*, **108**, 389–411.

Joos F, Prentice IC, Sitch S *et al.* (2001) Global warming feedbacks on terrestrial carbon uptake under the Intergovernmental

Panel on Climate Change (IPCC) emission scenarios. *Global Biogeochemical Cycles*, **15** (4), 891–907.

Kaminski T, Heimann M, Giering R (1999a) A coarse grid three-dimensional global inverse model of the atmospheric transport, part 1. A joint model and Jacobian Matrix. *Journal of Geophysical Research*, **104** (D15), 18535–18553.

Kaminski T, Heimann M, Giering R (1999b) A coarse grid three-dimensional global inverse model of the atmospheric transport, part 2. Inversion of the transport of CO_2 in the 1980s. *Journal of Geophysical Research*, **104** (D15), 18555–18581.

Kaplan JO (2001) *Geophysical Applications of Vegetation Modeling*. PhD Thesis, 128 pp. University of Lund.

Kaufmann MR, Troendle CA (1981) The relationship of leaf area and foliage biomass to sapwood conducting area in four subalpine forest tree species. *Forest Science*, **27** (3), 477–482.

Keeling CD, Whorf TP, Wahlen M *et al.* (1995) Interannual extremes in the rate of rise of atmospheric carbon dioxide since 1980. *Nature*, **375** (22 June 1995), 666–670.

Kicklighter DW, Bruno M, Dönges S *et al.* (1999) A first-order analysis of the potential role of CO_2 fertilization to affect the global carbon budget: a comparison of four terrestrial biosphere models. *Tellus*, **51B**, 343–366.

Kucharik CJ, Foley JA, Delire C *et al.* (1999) Testing the performance of a dynamic global ecosystem model: water balance, carbon balance, and vegetation structure. *Global Biogeochemical Cycles*, **14** (3), 795–825.

Kurz AD (1993) *Zur saisonalen Variabilität des ozeanischen Kohlendioxidpartialdrucks*. PhD Thesis, 107 pp. University of Hamburg.

Landsberg JJ, Gower ST (1997) *Applications of Physiological Ecology to Forest Management*. Academic Press, San Diego.

Larcher (1983) *Physiological Plant Ecology*, 303 pp. Springer, Heidelberg.

Lechowicz MJ, Hellens LE, Simon J-P (1980) Latitudinal trends in the responses of growth respiration and maintenance respiration to temperature in the beach pea, *Lathyrus japonicus*. *Canadian Journal of Botany*, **58**, 1521–1524.

Leemans R, Cramer W (1991) *The IIASA Database for Mean Monthly Values of Temperature, Precipitation and Cloudiness of a Global Terrestrial Grid*. RR-91-18. International Institute for Applied Systems Analysis (IIASA).

Leemans R, Prentice IC (1989) FORSKA, a general forest succession model. Meddelanden från Växtbiologiska Institutionen, Uppsala (ISSN 0348-1417), 1989: 2.

Lloyd J, Taylor JA (1994) On the temperature dependence of soil respiration. *Functional Ecology*, **8**, 315–323.

Maier-Reimer E (1993) Geochemical cycles in an ocean general circulation model – preindustrial tracer distributions. *Global Biogeochemical Cycles*, **7** (3), 645–677.

Malingreau J-P, Zhuang YH (1998) Biomass burning: an ecosystem process of global significance. In: *Asian Change in the Context of Global Climate Change* (eds Galloway J, Melillo J), pp. 101–127. Cambridge University Press, Cambridge.

Marland J, Boden TA, Griffin RC *et al.* (1989) Estimates of CO_2 emissions from fossil fuel burning and cement manufacturing, based on US Bureau of Mines manufacturing data. ORNL/CIAC-25, NDP-030, Carbon Dioxide Inf. Anal. Center. Oak Ridge National Laboratory, Oak Ridge, Tenn.

McGuire AD, Sitch S, Clein JS *et al.* (2001) Carbon balance of the terrestrial biosphere in the twentieth century: analyses of CO_2, climate and land use effects with four process-based ecosystem models. *Global Biogeochemical Cycles*, **15**, 183–206.

Meentemeyer V (1978) Macroclimate and lignin control of litter decomposition rates. *Ecology*, **59** (3), 465–472.

Melillo JM, McGuire AD, Kicklighter DW *et al.* (1993) Global climate change and terrestrial net primary production. *Nature*, **363** (May 20), 234–240.

Menzel L (1997) Modellierung der Evapotranspiration im System Boden-Planze-Atmosphäre. Zürcher Geographische Schriften Nr. 67, ETH.

Monsi M, Saeki T (1953) Über den Lichtfaktor in den Pflanzengesellschaften und seine Bedeutung für die Stoffproduktion. *Japanese Journal of Botany*, **14**, 22–52.

Monteith JL (1995) Accommodation between transpiring vegetation and the convective boundary layer. *Journal of Hydrology*, **166**, 251–263.

Neilson RP (1995) A model for predicting continental-scale vegetation distribution and water balance. *Ecological Applications*, **5** (2), 362–386.

New M, Hulme M, Jones PD (1999a) Representing twentieth century space-time climate variability. Part 1: development of a 1961–90 mean monthly terrestrial climatology. *Journal of Climate*, **12**, 829–856.

New M, Hulme M, Jones PD (1999b) Representing twentieth century space-time climate variability. Part 2: development of 1901–1996 monthly grids of terrestrial surface climate. unpublished.

Olson JS (1963) Energy storage and the balance of producers and decomposers in ecological systems. *Ecology*, **44** (2), 322–331.

Pacala SW, Canham CD, Silander JA (1993) Forest models defined by field measurements. I. The design of a northeastern forest simulator. *Canadian Journal of Forest Research*, **23**, 1980–1988.

Prentice IC, Cramer W, Harrison SP *et al.* (1992) A global biome model based on plant physiology and dominance, soil properties and climate. *Journal of Biogeography*, **19**, 117–134.

Prentice IC, Farquhar GD, Fasham MJR *et al.* (2001) The carbon cycle and atmospheric carbon dioxide. In: *Climate Change 2001: The Scientific Basis* (eds Houghton JT, Ding Y, Griggs DJ, Noguer M, van der Linden PJ, Xiaosu D). Cambridge University Press, Cambridge.

Prentice IC, Heimann M, Sitch S (2000) The carbon balance of the terrestrial biosphere: ecosystem models and atmospheric observations. *Ecological Applications*, **10** (6), 1553–1573.

Prentice IC, Leemans R (1990) Pattern and process and the dynamics of forest structure: a simulation approach. *Journal of Ecology*, **78**, 340–355.

Prentice IC, Sykes MT, Cramer W (1993) A simulation model for the transient effects of climate change on forest landscapes. *Ecological Modelling*, **65**, 51–70.

Prentice IC, Webb RS, Ter-Mikhaelian MT *et al.* (1989) Developing a global vegetation dynamics model: results of an IIASA summer workshop. IIASA Research Reports, 89 (7). International Institute for Applied Systems Analysis.

Raich JW, Rastetter EB, Melillo JM *et al.* (1991) Potential net primary productivity in South America: Application of global model. *Ecological Applications*, **1** (4), 399–429.

Reich PB, Walters MB, Ellsworth DS (1997) From tropics to tundra: global convergence of plant functioning. *Proceedings of the National Academic Science USA*, **94**, 13730–13734.

Robichaud E, Methven IR (1992) The applicability of the pipe model theory for the prediction of foliage biomass in trees from natural, untreated black spruce stands. *Canadian Journal of Forest Research*, **22**, 1118–1123.

Robock A, Vinnikov KY, Schlosser CA *et al.* (1995) Use of midlatitude soil moisture and meteorological observations to validate soil moisture simulations with biosphere and bucket models. *Journal of Climate*, **8**, 15–35.

Ryan MG (1989) Sapwood Volume for three subalpine conifers: predictive equations and ecological implications. *Canadian Journal of Forest Research*, **19**, 1397–1401.

Ryan MG (1991) Effects of climate change on plant respiration. *Ecological Applications*, **1** (2), 157–167.

Ryan MG, Binkley D, Fownes JH (1997) Age-related decline in forest productivity: Pattern and process. *Advances in Ecological Research*, **27**, 213–262.

Schoettle AW, Fahey TJ (1994) Foliage and fine root longevity of pines. *Ecological Bulletins*, **43**, 136–153.

Shinozaki K, Yoda K, Hozumi K *et al.* (1964a) A quantitative analysis of plant form-the pipe model theory I. *Japanese Journal of Ecology*, **14**, 97–105.

Shinozaki K, Yoda K, Hozumi K *et al.* (1964b) A quantitative analysis of plant form-the pipe model theory II further evidence of the theory and its application in forest ecology. *Japanese Journal of Ecology*, **14** (4), 133–139.

Shugart HH (1984) *A Thoery of Forest Dynamics*. Springer, New York.

Sitch S (2000) The role of vegetation dynamics in the control of atmospheric CO2 content. PhD Thesis, Lund University, Sweden.

Sitch S, Smith B, Prentice IC (2002) LPJ-DGVM a users manual. PIK report, unpublished.

Six KD, Maier-Reimer E (1996) Effects of plankton dynamics on seasonal carbon fluxes in an ocean general circulation model. *Global Biogeochemical Cycles*, **10** (4), 559–583.

Smith B, Prentice IC, Sykes MT (2001) Representation of vegetation dynamics in the modelling of terrestrial ecosystems: comparing two contrasting approaches within European climate space. *Global Ecology and Biogeography*, **10**, 621–637.

Smith TM, Shugart HH, Woodward FI eds (1997) In: *Plant Functional Types*, 369 pp. Cambridge University Press, Cambridge.

Specht RL (1970) Vegetation. In: *The Australian Environment* (ed. Leeper GW), pp. 44–67. CSIRO Australia and Melbourne University Press, Melbourne.

Specht RL (1972) Water use by perennial evergreen plant communities in Australia and Papua New Guinea. *Australian Journal of Botany*, **20**, 273–299.

Specht RL (1981) Growth indices – their role in understanding the growth, structure and distribution of Australian vegetation. *Oecologia*, **50**, 347–356.

Sprugel DG, Ryan MG, Renee Brooks J *et al.* (1995) Respiration from the organ level to the stand. In: *Resource Physiology of Conifers* (eds Smith WK, Hinckley TM), pp. 255–300. Academic Press, San Diego, California.

Steffen WL, Walker BH, Ingram JSI *et al.* (1992) *Global Change and Terrestrial Ecosystems. The Operational Plan*. Stockholm.

Thonicke K, Venevsky S, Sitch S *et al.* (2001) The role of fire disturbance for global vegetation dynamics: coupling fire into a Dynamic Global Vegetation Model. *Global Ecology and Biogeography*, **10**, 661–677.

Tjoelker MG, Oleksyn J, Reich PB (1999) Acclimation of respiration to temperature and CO_2 in seedlings of boreal tree species in relation to plant size and relative growth rate. *Global Change Biology*, **5** (6), 679–691.

VEMAP (1995) Vegetation/ecosystem modeling and analysis project: Comparing biogeography and biogeochemistry models in a continental-scale study of terrestrial ecosystem responses to climate change and CO_2 doubling. *Global Biogeochemical Cycles*, **9** (4), 407–437.

Venevsky S (2001) Broad-scale vegetation dynamics in north-eastern Eurasia – observations and simulations. PhD Thesis, Universität für Bodenkultur Wien.

Waring RH (1983) Estimating forest growth and efficiency in relation to canopy leaf area. *Advances in Ecological Research*, **13**, 327–354.

Waring RH, Schlesinger WH (1985) *Forest Ecosystems: Concepts and Management*. Academic Press, Orlando, Florida.

Waring RH, Schroeder PE, Oren R (1982) Application of pipe model theory to predict canopy leaf area. *Canadian Journal of Forest Research*, **12**, 556–560.

Woodward FI, Lomas MR, Lee SE (2000) Predicting the future production and distribution of global terrestrial vegetation. In: *Terrestrial Global Productivity* (eds Roy J, Saugier B, Mooney HA). Academic Press, San Diego.

Yoder BJ, Ryan MG, Waring RH (1994) Evidence of reduced photosynthetic rates in old trees. *Forest Science*, **40**, 513–527.

Zeide B (1993) Primary unit of the tree crown. *Ecology*, **74** (5), 1598–1602.

Zobler L (1986) A world soil file for global climate modelling. *NASA Technical Memorandum*, **87802**, 32.

Appendix: estimation of soil temperature

The seasonal cycle of surface air temperatures is assumed to approximate a sinusoid. Soil temperature follows the surface air temperature cycle with a damped oscillation about a common mean, and a temporal lag. The soil temperature, T_{soil} at depth z at time t (Campbell & Norman, 1998) is given by:

$$T_{\text{soil}}(z,t) = T_{\text{ave}} + A \cdot \exp\left(\frac{-z}{d}\right) \sin\left(\Omega t - \frac{z}{d}\right) \qquad \text{(A1)}$$

where T_{ave} is average surface air temperature over the last 12 months, A is the amplitude of the air temperature fluctuation and

$$d = \sqrt{\frac{2k}{\Omega}}, \quad \Omega = \frac{2\pi}{\tau} \qquad \text{(A2)}$$

where d represents the damping depth, τ the oscillation period (here set to 12 months) and Ω the angular frequency of oscillation. In a physical sense, $\exp(-z/d)$ expresses the fractional amplitude of temperature variation at soil depth z, relative to the surface temperature fluctuation, in essence a damping term; z/d represents the oscillation lag of the soil at depth z relative to the

surface, in angular units; k is the soil texture dependent thermal diffusivity. Soil thermal diffusivities are moisture dependent and a function is created by linear interpolation between estimates for 0% (k_0), 15% (k_{15}) and 100% (k_{100}) soil water content from Campbell & Norman (1998) (Table 4). Soil temperatures are calculated at 0.25 m depth, i.e. half the depth of the upper soil layer since the majority of the readily decomposable organic material resides in the uppermost soil horizons. Combining Eqs (A1) and (A2) and estimating the lag in air temperature ('lag' months from present) by linear interpolation between air temperatures from this month and the last gives:

$$
\begin{aligned}
T_{\mathrm{soil}}(m) = & \left(\sum_{n=m-11}^{m} \frac{T_{\mathrm{air}}(n)}{12} \right) \\
& + A_{\mathrm{frac}} \left[T_{\mathrm{air}}(m) - T_{\mathrm{air}}(m-1)(1-\mathrm{lag}) \right. \\
& \left. + T_{\mathrm{air}}(m-1) - \left(\sum_{n=m-11}^{m} \frac{T_{\mathrm{air}}(n)}{12} \right) \right] \\
A_{\mathrm{frac}} = & \, e^{\left(\frac{-z}{d}\right)} = e^{\left(\frac{1}{8}\sqrt{\frac{\pi}{3\kappa}}\right)} \\
\mathrm{lag} = & \frac{z}{d} \frac{12}{2\pi} = \left(\frac{1}{4} \sqrt{\frac{3}{\kappa\pi}} \right)
\end{aligned}
\tag{A3}
$$